ANL-6657
Chemistry
(TID-4500, 19th Ed.)
AEC Research and
Development Report

ARGONNE NATIONAL LABORATORY
9700 South Cass Avenue
Argonne, Illinois

A STUDY OF THE THERMODYNAMIC PROPERTIES OF THE VANADIUM-IRON ALLOY SYSTEM

by

Kevin Michael Myles

Metallurgy Division

Metallurgy Program 4.10.32

Portions of the material included in this report have appeared in the following Metallurgy Division progress report:

ANL-6516 pp. 267-268 December 1961

February 1963

Operated by The University of Chicago
under
Contract W-31-109-eng-38
with the
U. S. Atomic Energy Commission

DISCLAIMER

TABLE OF CONTENTS

LIST OF FIGURES

LIST OF FIGURES

LIST OF TABLES

A STUDY OF THE THERMODYNAMIC PROPERTIES OF THE VANADIUM-IRON ALLOY SYSTEM

by

Kevin Michael Myles

ABSTRACT

The vapor pressure of iron over vanadium-iron alloys has been measured by the torsion-effusion method in the temperature range from 1500 to 1700°K. The chemical activities, as well as the free energies, entropies, and enthalpies of formation, of the alloys have been computed from the vapor pressure data.

The activities of iron exhibit large negative deviations from Raoult's law throughout the entire compositional range. Although the activities of vanadium, as determined by the Gibbs-Duhem relation, deviate negatively from ideal behavior in the iron-rich alloys, nearly ideal behavior is observed in the vanadium-rich alloys.

Large positive excess entropies and enthalpies of formation are found at 1600°K. An attempt is made to interpret these quantities in terms of the various configurational, vibrational, and magnetic changes that occur in this system upon alloying.

INTRODUCTION

An ultimate goal of alloy chemistry is the development of a general theory which would enable the prediction of the structure and properties of an alloy from a similar knowledge about its component elements. There have been two rather distinct approaches toward this goal. The atomistic approach involves the analysis of electronic and crystalline structures, whereas the macroscopic point of view is concerned with the interpretation of thermodynamic properties. Although these involve entirely different disciplines, it is essential that any hypothesis derived while following one be consistent with conclusions drawn while following the other. It is unfortunate that during the past several decades many more contributions have been made with the atomistic approach than have been made with the macroscopic.

It is the object of this research to partially reduce this deficit by determining the thermodynamic properties of the vanadium-iron alloy system and to attempt to interpret these data in terms of the various configurational, vibrational, and magnetic changes that occur in this system upon alloying.

The thermodynamic properties of paramount interest in alloy chemistry, namely, the Gibbs free energy F, the enthalpy H, and the entropy S, are related by the Gibbs-Helmholtz relation

$$F = H - TS \quad . \tag{1}$$

For the particular case of an isothermal reaction involving the formation of an alloy from its component elements, Equation (1) becomes

$$\Delta F = \Delta H - T\Delta S \quad , \tag{2}$$

where ΔF, ΔH, and ΔS represent the changes occurring in the free energy, enthalpy, and entropy accompanying the formation.

The free energy of formation of the alloy is interpreted as a quantitative measure of its stability relative to its pure components and describes most completely the concept of a "driving force" for the formation. The enthalpy of formation is a measure of the heat evolved or absorbed during the reaction. The entropy of formation, although not easily defined, is of particular interest since it can be directly related to modifications in the atomic, electronic, or magnetic configuration of the components upon alloying.

In general, the experimental techniques used to determine these thermodynamic quantities may be divided into two categories: (1) those that employ a reaction calorimeter for the determination of ΔH or a drop calorimeter for the determination of ΔS,(1) and (2) those that evaluate ΔF by some suitable equilibrium method. Unlike the calorimetric techniques, which may be used for the determination of only one of the three thermodynamic quantities, the equilibrium methods, in principle, permit the determination of all three. In practice, however, the values of ΔS and ΔH so obtained are generally less accurate than those obtained calorimetrically. This apparent ability to survey all three thermodynamic quantities was consistent with the objective of this research. The two equilibrium quantities that have generally proven to be the most satisfactory for the determination of thermodynamic properties are the electromotive force and the vapor pressure.

The electromotive-force method is considered to be more precise than any of the vapor pressure methods;(2) but because of subtle conditions, which may produce interfering side reactions in a given galvanic cell, the

accuracy is often considerably lower. The galvanic cell contains an electrode of the alloy under study and an electrode of the less noble component of the alloy immersed in an electrolyte containing ions of the less noble component. Under the condition that the cell reaction tends reversibly toward equilibrium, the free energy of formation of the alloy is given by the relationship

$$\Delta F = - n\ 23066E \quad . \tag{3}$$

Here, 23066 is the Faraday constant expressed in calories/volt, n the number of faradays that pass if the reaction goes to completion, and E the electromotive force expressed in volts.

In adapting this experimental technique to alloy systems, care must be taken to insure that only the reaction under consideration produces the measured emf. As a consequence, no localized concentration changes may occur during the course of the measurement. Hence, to investigate solid alloys, the diffusion rate of the transported ion into the electrode must be great enough to avoid changes in composition at the electrode-electrolyte interface. In most cases, the temperatures required for adequate diffusion rates place severe limitations on the number of suitable electrolytes. If the metal anion of the electrolyte has more than one valence state, precautions must be taken to insure that only one known state is present. Furthermore, the affinity of the anion for the more electropositive component must be much less than its affinity for the other component; otherwise, the emf created in the cell will be very small and, as a result, difficult to measure. Hence, the emf method is likely to be unsatisfactory with binary alloys whose components are close to one another in the electromotive series. The problems of obtaining a satisfactory electrolyte are most acute for alloys of the transition metals; as a consequence, it appeared that vapor pressure measurements would be experimentally better suited to this present research.

Vapor pressure methods to determine thermodynamic data are based on the relationship

$$\Delta F = RT \ln (p/p^\circ) \quad , \tag{4}$$

where p and p° represent the vapor pressure of the more volatile component in the alloyed and pure state, respectively. The experimental methods generally employed for measuring these vapor pressures fall into two categories, depending upon the magnitude of the pressures involved, and have been extensively reviewed by previous workers.[2-4] The high-pressure (10^3 to 10^{-2} mm Hg) methods include the use of such static devices as manometers, Bourdon gauges, and isoteniscopes. Boiling point determinations, weight displacements, and dew-point evaluations have been used to measure the vapor pressure in this pressure range. The principal

dynamic method is the entrainment method in which the pressure is determined from the density of an inert gas and metal vapor stream in equilibrium with the metal surface. The low-pressure (10^{-2} to 10^{-8} mm Hg) methods are, in general, dynamic and involve an evaluation of the rate of evaporation or sublimation of a specimen into a vacuum.

Since the quantity of metal transferred from a condensed phase at a given temperature is directly proportional to the vapor pressure and the time, metals with extremely low vapor pressures can be sublimed over long periods to provide measurable weight changes from which the vapor pressures can be calculated. Most of these methods are variants of those developed by Langmuir[5] and Knudsen,[6,7] and have been discussed in detail previously.[2,4,8]

In the Langmuir method, an exposed specimen is heated in a vacuum, and the rate of sublimation or evaporation is measured. An estimation of the fraction of the sublimed atoms that are deflected back to the sample surface and condensed must in all cases be made by comparison measurements with other methods.

Unambiguous determinations of the vapor pressure may be made with the Knudsen method, in which the metallic specimen is enclosed in a cell provided with a small orifice. The vapor, which at a given temperature is in equilibrium with the sample, flows through the orifice into a region of high vacuum. Based on the kinetic theory of gases, the relationship between the equilibrium vapor pressure and the mass m of a vapor effusing through an orifice with a negligible thickness and area A in a time t is given by

$$p = \frac{m}{tA}\sqrt{\frac{2\pi RT}{M}} \quad , \tag{5}$$

where M is the molecular weight of the vapor. To insure that the rate of effusion per unit orifice area, m/tA, is directly proportional to the pressure inside the cell, Knudsen has shown that the ratio of the mean free path of the effusing atoms in the vapor to the radius of the orifice must be greater than 10. This condition sets an upper limit of about 10^{-2} mm Hg to the pressure range over which the method may be employed. The lower limit is determined by the accuracy with which the weight of evaporated material can be measured after a run of reasonable duration.

The assumption is made in Equation (5) that the pressure within the Knudsen cell is the equilibrium vapor pressure of the specimen and hence is not perturbed by the orifice openings. Whitman[9,10] suggests that equilibrium pressures can never exist because the relatively slow molecular flow at the low pressures involved does not permit the attainment of a steady state. On the other hand, Speiser[8] concludes that the

cell equilibrium is not disturbed by the orifice openings when the ratio of the orifice area to the effective surface area of the specimen is considerably smaller than unity. This condition insures that the rate of sublimation is much greater than the rate of effusion.

Another factor that must be considered is the resistance to the flow of the vapor from the cell produced by the finite thickness of the orifice walls. Clausing[11,12] investigated this problem and deduced corrections to Equation (5) based on the ratio of orifice length to orifice area.

As an alternative to the determination of the rate of effusion by the weight-loss technique, a radioactive isotope of the specimen may be condensed on a collector plate. The intensity of the radioactivity is related to the weight of effused material. The advantages of this modification are that smaller weight changes can be measured accurately, which in turn extends the range to lower pressures, and that less time is required to obtain a reproducible determination of the effusion rate. This latter factor is quite important in alloy investigations because it minimizes the possibility of compositional changes during the course of the experiment. Care must be exercised to eliminate errors that arise from either incomplete condensation or resublimation of the effusant.[2,8] In addition, a correction must be made for the difference in mass between the radioactive isotope and the natural mixture of isotopes.

An ingenious variation of the Knudsen method, the torsion-effusion method,[13-15] consists of an effusion cell suspended by a fine wire. The effusion cell is constructed so that a torsional force is developed in the wire as the vapor effuses in a horizontal direction through two eccentrically placed orifices. The angle of rotation through which the cell moves is related to the vapor pressure in a simple way. The two great advantages of this method are that it is more rapid than even the refined Knudsen techniques, and it is unnecessary to know the atomicity of the vapor. Corrections similar to those deduced by Clausing for the Knudsen method must be made for the reduction in effective force of the effusing vapor caused by the nonzero lengths of the orifices. These corrections have been calculated by Freeman and Searcy[16,17] and by Detkov[18] with similar results.

Since the work included in this research was to be but a part of a program designed to survey and compare the thermodynamic properties of a wide variety of transition metal alloys, an experimental method was required that could best meet this overall objective. The torsion-effusion method appeared to have the suitable characteristics and the wide applicability needed for this program.

The vanadium-iron alloy system was chosen as the subject of this research because a large amount of pertinent information, derived by other experimental means, was available and presumably would greatly assist in the interpretation of the thermodynamic data. The extensive range of solid solubility as illustrated by its phase diagram shown in Figure 1 permitted the determination of the thermodynamic properties over the entire alloy system. Further, this system appeared to be suited to vapor pressure measurements by the torsion-effusion method since the vapor pressure of iron was reported to be about two orders of magnitude larger than that of vanadium. This allowed the partial pressures of iron vapor over the alloys to be easily measured in the presence of the vanadium vapor.

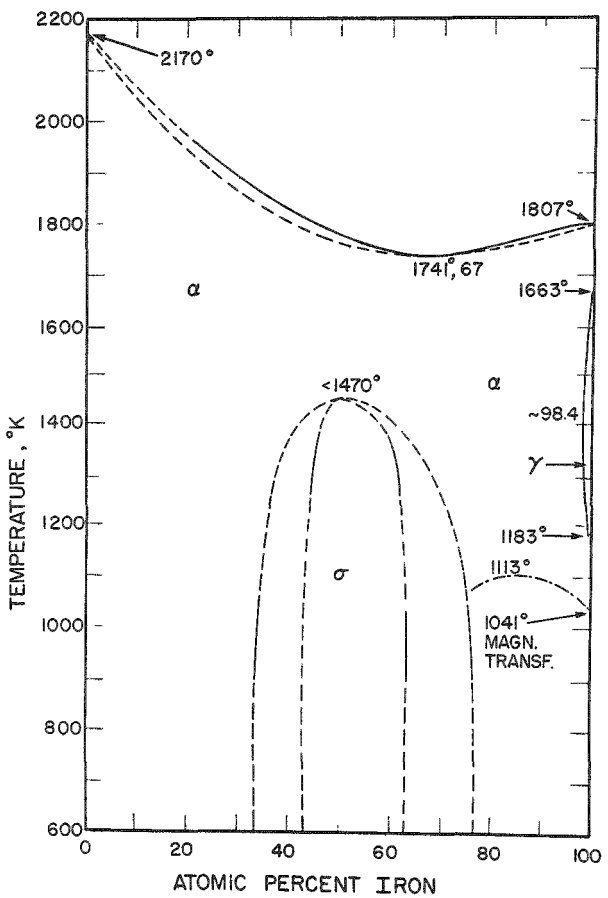

Figure 1. The Vanadium-Iron Equilibrium Diagram after Hansen[19]

EXPERIMENTAL TECHNIQUES

The torsion-effusion method as first developed by Mayer[13] and Volmer[14] has subsequently been used by a large number of workers.[15,16,20-34] The efforts of several of these workers are noteworthy with regard to the present work. Wessel[26] determined the vapor pressure of iron by employing effusion cells of quartz and alumina suspended from a tungsten torsion wire in a graphite sheath furnace capable of operating at temperatures up to 1500° C. This temperature range was extended to 1900° C by Searcy and Freeman[27] with induction heating. Unfortunately, the latter workers experienced a rotational electromagnetic coupling between the cell and the field of the heater coil. A null-point apparatus has been developed by Rosen[35] that eliminates those errors which might arise from changes in the torsion constant of the wire or from hysteresis effects. The first workers to use the torsion-effusion method to study the thermodynamics of alloys were Aldred and Pratt.[33]

Design of Apparatus

The design of the apparatus employed in the present work is similar to that described by Pratt and Aldred.[36] The apparatus consists of a torsion system that is suspended inside a vertical vacuum chamber whose lower end is surrounded by a high-temperature vacuum furnace. An optical lever and scale are used to measure the degree of rotation of the effusion cell. The apparatus is shown diagrammatically in Figure 2 and pictorially in Figure 3.

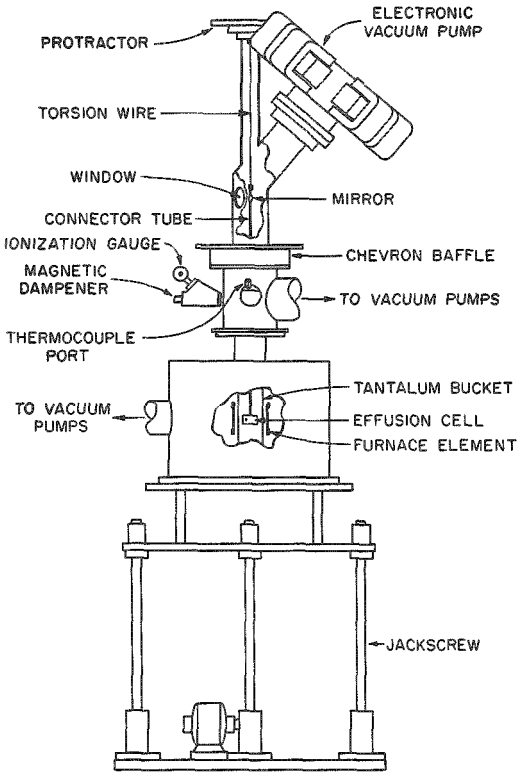

35706

Figure 2a. Schematic of the Torsion-Effusion Apparatus

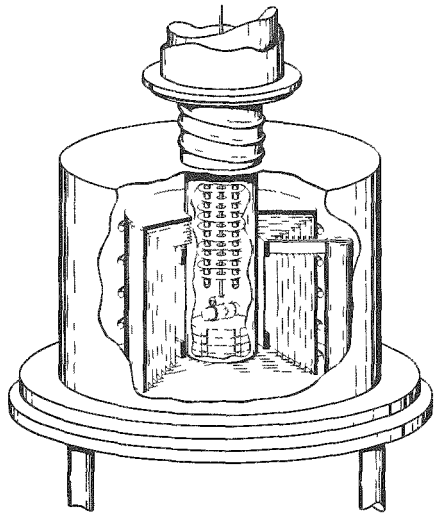

35705

Figure 2b. Lower Portion of the Torsion-Effusion Apparatus

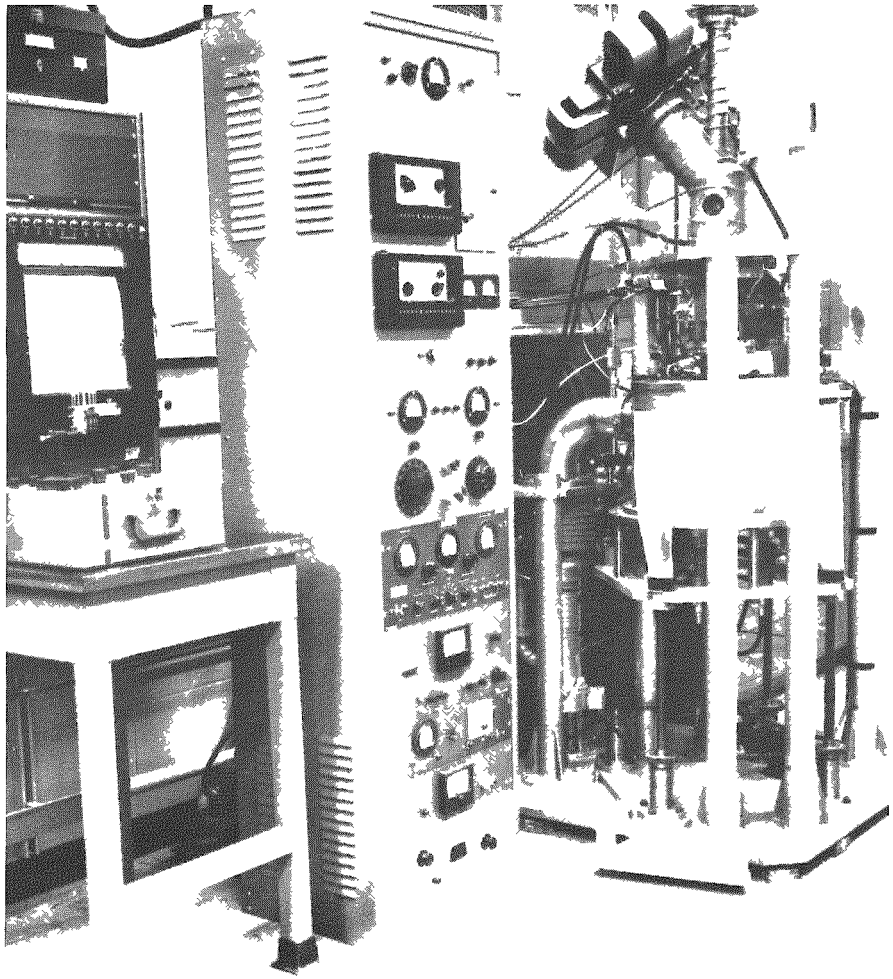

34211

Figure 3a. Front View of the Torsion-Effusion Apparatus

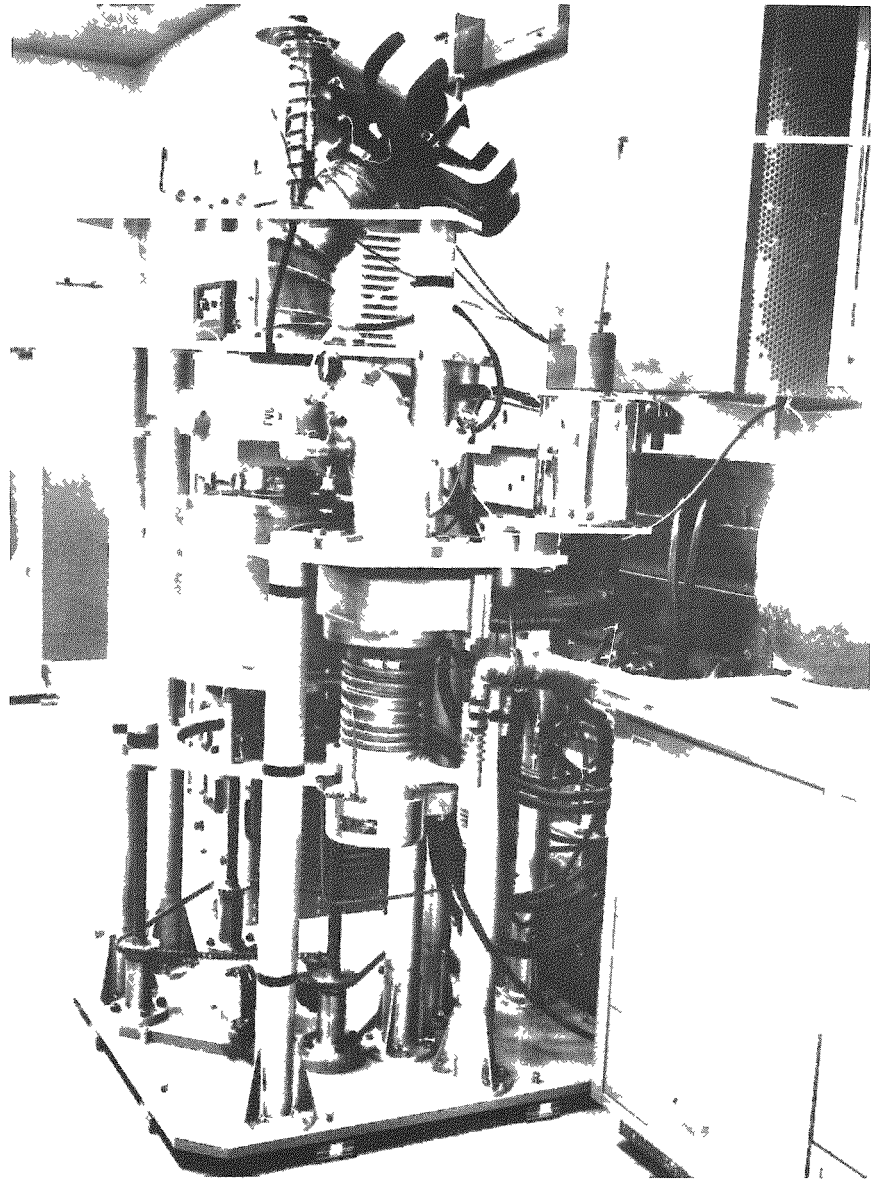

34207

Figure 3b. Rear View of the Torsion-Effusion Apparatus

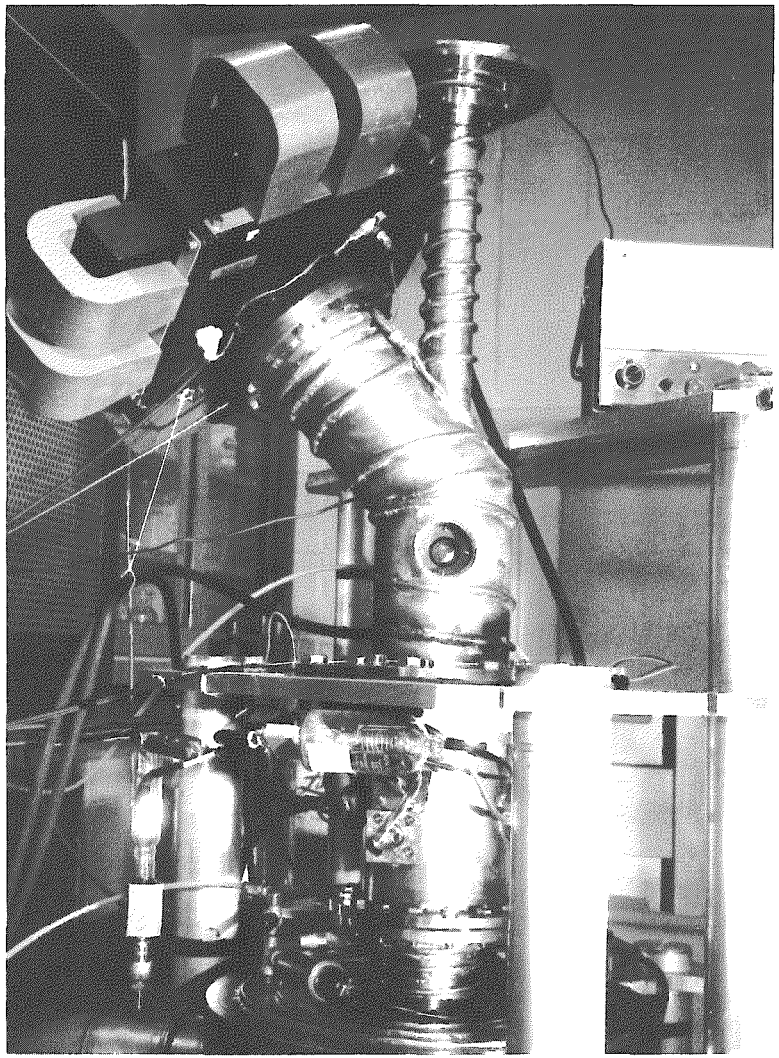

34209

Figure 3c. Upper Portion of the Torsion-Effusion Apparatus

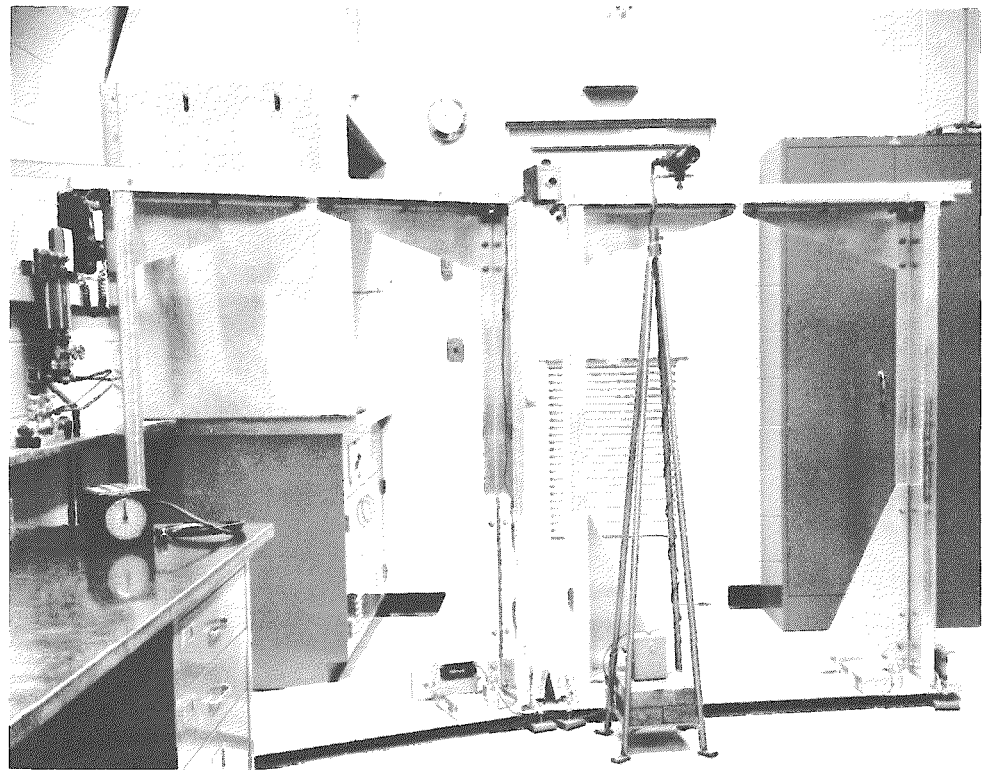

34206

Figure 3d. View of the Scale of the Torsion-Effusion Apparatus

At the top of the torsion system a protractor, shown in Figure 3c, is mounted so that the torsion system can be rotated in units of one minute of arc. Fastened immediately below the protractor, but electrically insulated from it, is a small chuck, which holds the torsion wire. The torsion wire is an annealed, high-purity, tungsten wire usually between 0.001 and 0.002 in. in diameter and about 17 in. in length. To the bottom end of the torsion wire is attached another chuck that supports a mirror and a thin-walled, tantalum connector tube, which is $\frac{1}{8}$ in. in diameter and 25 in. long. The mirror is a front-surface, galvanometer type, which is ground concave with a radius of curvature of 4 m. The effusion cell is connected to the lower end of the tantalum tube as shown in Figure 2b.

The upper portion of the vacuum chamber, seen in Figure 3c, is a 2-in.-diameter tube, which surrounds the torsion wire. Welded to this tube, forming a wye section, is a 4-in.-diameter tube, which supports an electronic high-vacuum pump with a pumping speed of 90 liters/sec. In the vertical portion of the wye section is a port fitted with an optically flat glass window of low index of refraction, which is $1\frac{1}{8}$ in. in diameter by $\frac{1}{8}$ in. thick. Beneath the wye section, is an aluminum, chevron baffle, shown in Figure 2a, which has been modified by carefully positioning a vertical tube at the center of the bolt circle of the baffle. A double-walled, water-cooled tee section, which is connected to the underside of the baffle, is fitted with ports for two thermocouple seals and an assembly which consists of an electromagnetic dampener and a hot-cathode ionization gauge. The electromagnetic dampener, wound on a silicon-iron core, produces a field of around 300 gauss at full current. As a precaution against the possibility that the dampener might alter the zero point or restrict the rotational motion of the torsion system, a provision is made to withdraw and rotate the dampener poles 90° from the aluminum dampener vane that is positioned on the connector tube. All of the demountable joints in the vacuum chamber are sealed with "Viton" O-rings. Except where noted, the vacuum chamber is constructed of austenitic stainless steel. A high-vacuum gate valve, bolted to the horizontal leg of the tee section, separates the vacuum pump system and the vacuum chamber. The vacuum pump system, shown in Figure 3b, includes a chevron-baffle cold-trap, a 5-in., four-stage, fractionating diffusion pump with a pumping speed of 750 liters/sec, and a two-stage forepump with a pumping speed of 425 liters/min. Extending from the bottom of the tee section, as shown in Figure 2b, are two, thin-walled, tantalum, thermocouple-protection wells that support tantalum heat reflectors. The latter are separated by recrystallized alumina spacers. Surrounding this assembly, which consists of the thermocouple wells and the heat reflectors, and the effusion cell is a tantalum bucket, which forms the terminal portion of the vacuum chamber and is $2\text{-}\frac{1}{8}$ in. in diameter and about 16 in. long. Additional heat reflectors are located at the bottom of the tantalum bucket beneath the effusion cell.

The vacuum furnace, shown in Figure 2b, is a noninductive, high-temperature, sheath type. The single-phase, tubular, tantalum heating element is $2\text{-}\frac{1}{2}$ in. in diameter, 6 in. high, and 0.005 in. thick, and is designed

with a vertical free-floating suspension which allows for the unrestricted downward movement of the element caused by thermal expansion upon heating. Seven cylindrical tantalum heat reflectors and a water-cooled copper heat shield completely surround the element on the sides, top, and bottom. Power is supplied to the element by means of three vacuum-tight, water-cooled, electrical feed-throughs. The entire furnace assembly is enclosed within a stainless steel bell jar that is connected to a high-vacuum system. This vacuum system consists of a 4-in. water-cooled baffle, a 4-in., three-stage, fractionating diffusion pump with a pumping speed of 300 liters/sec, and a two-stage forepump with a pumping speed of 375 liters/min. The bell jar may be lowered away from the vacuum chamber by operating four screw jacks. The electrical power system, shown in Figure 3b, includes a 17-kva, 208/1/60, self-saturating saturable core reactor with an integral magnetic amplifier and a water-cooled, 15-kva, 208/1/60 primary stepdown power transformer with a multitap secondary. The furnace-control system, shown in Figure 3a, consists of a reference voltage source with a 0-20 millivolts range, a dc electronic null detector, a current-adjusting proportional band relay, and the self-saturating reactor described above. A platinum-platinum-10 per cent rhodium thermocouple, which was insulated with recrystallized alumina and positioned in one of the thermocouple protection wells, is used as the temperature-sensing device. The temperature range over which the furnace has been calibrated with this thermocouple is from 700 to about 1600° C. The maximum attainable furnace temperature is about 2200° C.

The scale for the optical lever, shown in Figure 3d, is a flexible 10-ft steel rule graduated in hundreths of an inch. The rule is supported at the same elevation as the light source and mirror by an aluminum stand. The aluminum stand is constructed and positioned so that the scale forms an arc of a circle 4 m in radius, whose center coincides with the axis of the torsion system.

Both the scale and the vacuum chamber-furnace assemblies are mounted on vibration eliminators to reduce any disturbance of the torsion suspension by external vibrations. In addition, rubber connections are used between the diffusion and forepumps, and for all water lines.

Tantalum end caps are electron-beam welded to a 0.010-in.-wall tantalum tube to produce an effusion cell, which is $\frac{1}{2}$ in. in diameter by $1\frac{3}{4}$ in. long, shown in Figure 4. The two effusion orifices, formed by drilling, may have diameters from $\frac{3}{64}$ in. to $\frac{5}{64}$ in., depending upon the magnitude of the vapor pressure to be measured. A carefully matched tantalum yoke and harness, which dovetailed to facilitate assembly and disassembly, are used to fasten the cell to the connector tube. Circumferential and lateral lines are scribed on the cells, the yoke, and the harness to define relative orientations during assembly.

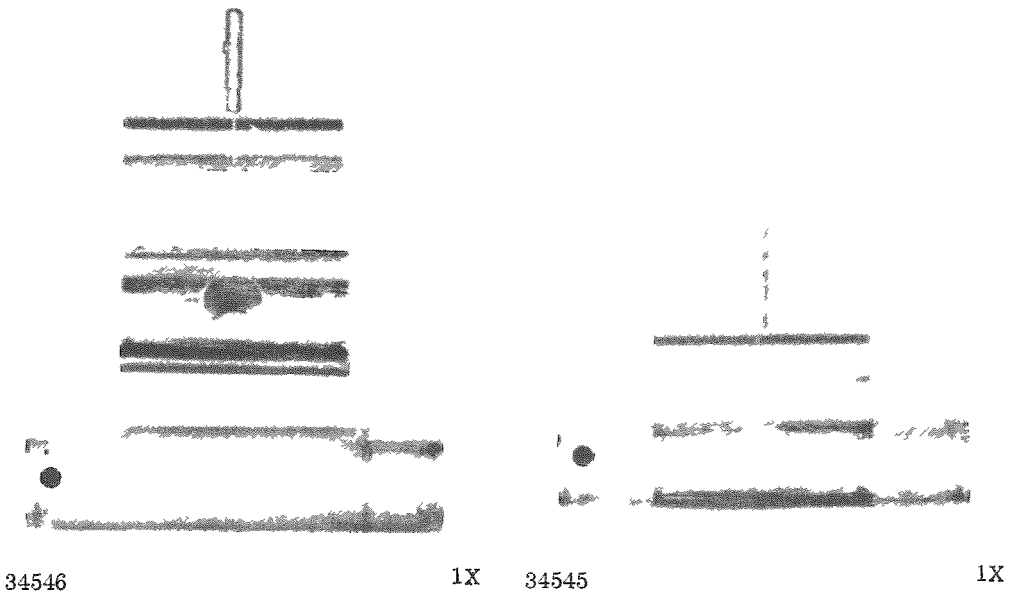

Figure 4. Exploded and Assembled Views of an Effusion Cell, Yoke, and Harness

Evaluation and Calibration

After the initial assembly and check-out of the apparatus was completed, evaluations were made of the furnace control and the hot-zone gradients. In evaluating the furnace control, a platinum-platinum-10 per cent rhodium thermocouple was inserted into a dummy effusion cell, filled with tantalum scrap to simulate a specimen, and located in the normal cell position. The emf output of the thermocouple was monitored with a self-balancing potentiometer. The evaluation showed that the furnace had a temperature-control stability of $\pm\frac{1}{2}$° C at 1300° C. With a similar experimental arrangement, the vertical temperature variation over the $2\frac{1}{2}$-in. hot zone was found to be ±3° C at 1450° C and, within the cell, ±1° C. Simultaneous readings of three thermocouples placed in the dummy cell indicated that the horizontal temperature variation across the cell was $\pm\frac{3}{4}$° C at 1350°C.

With the above evaluations complete, calibrations of the working thermocouple, the light screen, and the torsion wire were undertaken. The working and secondary standard thermocouples were made from 24-gauge, thermocouple-grade platinum-platinum-10 per cent rhodium wire. After the wires were beaded and insulated with recrystallized alumina, they were annealed at white heat for about one hour. The working couple was subsequently enclosed in the remaining thermocouple-protection well to prevent contamination by the effusing metallic vapor and positioned in the furnace. The emf output from this thermocouple could be measured with either a multirange, null-point, millivolt recorder or a high-precision millivolt potentiometer. Since it was impossible to permanently attach the working

couple to the cell, as this would impede its free rotation, the couple was placed as near as possible to the cell, as shown in Figure 2b. A calibration was then made to relate the actual cell temperature, as determined by a secondary standard thermocouple positioned in the cell, to the emf produced across the working couple. The secondary standard thermocouple was calibrated against a primary standard couple that had been previously calibrated by the National Bureau of Standards. The results of the first two of these calibrations were evaluated by the least-squares method and then combined algebraically with the third to produce an overall cell temperature calibration expressed by the equation

$$E = 6.0172 + 11.4296 \times 10^{-3}T + 2.563 \times 10^{-7}T^2 \quad , \qquad (6)$$

where E is the measured emf in millivolts and T is the temperature of the cell in degrees Kelvin.

In order to confirm this calibration, small pieces of pure iron or nickel sheet were welded to the ends of a thermocouple that was positioned in the dummy cell and heated under experimental conditions. The melting point of the iron or nickel sheet was detected by the sudden interruption of the emf as the metal melted. The emf produced across the working couple was measured simultaneously with this interruption. It was found that the melting temperature of the two metals agreed to within 2° C with the accepted published values.

The scale was calibrated to determine the displacement of the reflected image of the hairline in the light source of the optical lever for a given rotation of the effusion cell. To facilitate this calibration, the torsion suspension was removed from the vacuum chamber and the torsion wire replaced by a rigid rod. Rotation of the calibration protractor effected a defined rotation of the mirror, which in turn caused the reflected image of the hairline to move along the screen. Repetitive rotations of the protractor, through arbitrary but known angles, showed that within experimental accuracy a rotation of one degree of the protractor resulted in the same displacement of the hairline image along the scale regardless of the point of origin. This calibration resulted in the relationship that

$$1° \text{ rotation of mirror} = 5.49 \text{ in. of displacement of light beam.} \qquad (7)$$

Before and after each experimental run it was necessary to determine the torsion constant, that is, the torque required to produce a unit angle of twist in the torsion wire. This constant τ was determined by periodicity measurements involving the relationship[37]

$$\tau = \frac{4\pi^2 I}{T_1^2 - T_2^2} \quad . \qquad (8)$$

Here, I is the moment of inertia of a removable portion of the torsion suspension, T_1 the period of oscillation of the torsion suspension with this portion in place, and T_2 the period of oscillation of the torsion suspension without this portion in place. To establish these parameters, the effusion cell, the yoke, and the harness were removed from the torsion suspension and replaced by the stainless steel tie-bar and cylinder of known moment of inertia, shown in Figure 5. The moment of inertia I of the cylinder was calculated by means of the relationship

$$I = M(d_1^2 + d_2^2)/8 \quad , \qquad (9)$$

where M is the mass, d_1 is the outside diameter of the cylinder, and d_2 is the inside diameter. In the present case, M = 45.6841 gm, d_1 = 1.8747 in., and d_2 = 1.7497 in.; hence, I = 242.27 gm-cm^2. The average periods were determined by setting the torsion suspension into motion for a minimum of 15 complete oscillations, counted by means of a photoelectric counter, and by measuring the elapsed time with the stop clock, shown in Figure 3d. Typical values for T_1 and T_2 for a 0.0015-in.-diameter torsion wire were 115.85 sec and 21.95 sec, respectively, which, when substituted into Equation (8), gave a torsion constant of 0.7392 dyne-cm/rad.

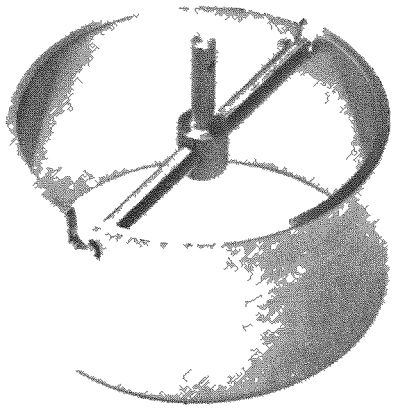

34548 1X

Figure 5. View of the Stainless Steel Tie-Bar and Cylinder

Operation

Prior to the experimental runs, the effusion cells were loaded and sealed with clean, preweighed specimens, which were machined in the form of loosely packed turnings to insure a large surface-to-volume ratio. The cells were then stored under acetone. As needed, a cell was removed from the acetone, washed with alcohol, and dried. The orifices were then photographed with a Baush and Lomb metallograph at 40 magnification. The areas of the photographic images of the orifices (see Figure 6) was subsequently determined with an Ott planimeter. The moment arms of the cell were measured with a traveling microscope, calibrated in thousandths of a millimeter. The effusion cell was weighed and fastened to the bottom of the torsion suspension, and the furnace assembly was raised into position. Both the furnace and the vacuum chamber were purged with argon gas and evacuated to a pressure of about 5 x 10^{-4} mm Hg as gently as possible to prevent any undue disturbance of the torsion suspension. After this pressure had been realized, the furnace temperature was raised to about 300° C to aid in out-gassing the cell. When the pressure in the vacuum chamber

was about 6 x 10^{-7} mm Hg, the electromagnetic dampener was withdrawn from around the suspension and the zero point of the system noted. The furnace controller was then reset to approximately 400° C and the zero point redetermined. If these two zero points were in agreement, the temperature of the cell was elevated to the desired experimental temperature.

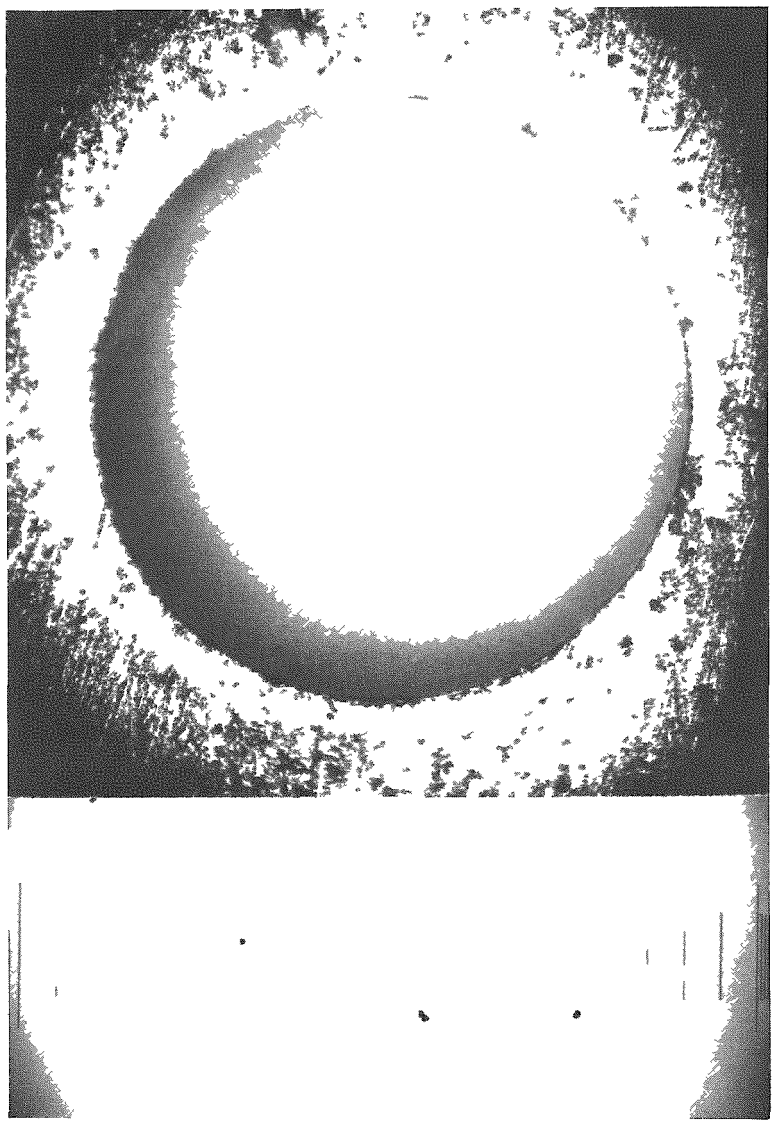

34348 and 34346 40X

Figure 6

Print of a Typical Negative of an Effusion Orifice and of the Graduated Scale Used in Determining the Magnification of the Negative

After the furnace had come to thermal equilibrium, as noted on the millivolt recorder, the rotation of the cell was measured. Care was taken to insure that this rotation was a steady-state value and thus representative of the equilibrium vapor pressure of the bulk specimen. The temperature was then raised and a new deflection noted; the entire cycle required about 15 min. Checks of electrical continuity were made throughout the experimental run with a vacuum-tube ohmmeter to ensure that neither the effusion cell nor the torsion suspension were touching the vacuum chamber and thereby impeding their free rotation. At the conclusion of the run, the

furnace was cooled, and the cell removed and reweighed. In general, the weight loss of the specimen did not exceed 0.2 per cent, which suggests that little change in the bulk alloy composition occurred during any of the runs. Spectrochemical analyses of several iron samples that were handled in a manner identical with that of the experimental specimens indicated that the tantalum pick-up from the cells was less than 10 ppm.

Chemical analyses indicated that the concentration of vanadium in the effusate was less than 0.1 per cent.

Specimen Preparation

The iron used in the present investigation was obtained from the Metals Manufacturing Control Laboratory, who indicated that the metal was 99.9635 per cent pure iron. The vanadium metal was 99.884 per cent pure according to its supplier, the Union Carbide Metal Company. The major impurities in the vanadium were carbon, nitrogen, oxygen, and hydrogen.

The specimens were cast in a tungsten arc furnace under a helium-argon atmosphere. Chemical analyses of the as-cast alloys were made for vanadium and iron contents. Chemical analyses for oxygen and nitrogen indicated that the alloys contained, at most, 670 ppm oxygen and 474 ppm nitrogen. The specimens were given a 3-hr homogenization and degassing heat treatment at 1450° C prior to each experimental run.

Effusion-cell Data

Table I lists the nominal alloy compositions, the analyzed alloy compositions, the moment arms d, the orifice areas A for the cells used in this work, and the Freeman-Searcy correction factors f to compensate for

Table I

EFFUSION-CELL CHARACTERISTICS

Cell	Alloy Composition		Moment Arms		Orifice Areas		Freeman-Searcy Correction Factors	
	Nom (a/o Iron)	Anal (a/o Iron)	d_1 (cm)	d_2 (cm)	A_1 ($cm^2 \times 10^2$)	A_2 ($cm^2 \times 10^2$)	f_1	f_2
Ta 3	100	100	2.0407	2.0158	1.9192	1.9490	0.8890	0.8898
Ta 5	100	100	2.0124	2.0359	3.1193	3.0626	0.9114	0.9107
Ta 6	90	91.3	2.0368	2.0207	2.0028	2.0563	0.8912	0.8925
Ta 7	80	80.7	2.0278	2.0314	2.0168	2.0539	0.8915	0.8924
Ta 8	70	70.4	2.0174	2.0393	2.0301	2.0512	0.8918	0.8923
Ta 9	60	59.6	2.0310	2.0299	2.0337	2.0374	0.8919	0.8920
Ta 10	50	50.1	2.0327	2.0297	2.0039	2.0065	0.8912	0.8913
Ta 11	40	39.9	2.0242	2.0261	2.0507	2.0757	0.8923	0.8929
Ta 12	30	30.4	2.0400	2.0337	2.8083	2.0855	0.9069	0.8932
Ta 13	20	20.6	2.0205	2.0376	2.0954	2.0176	0.8938	0.8915
Ta 14	10	9.5	2.0272	2.0352	2.0572	2.0529	0.8925	0.8924

the nonzero lengths of the orifices. Both the values of the moment arms and orifice areas were corrected for the effect of thermal expansion at any given temperature T by the use of the thermal expansion coefficient α for tantalum:[38]

$$\alpha = 5.6435 \times 10^{-6} + 1.50 \times 10^{-9}T \quad . \tag{10}$$

The cell-wall thicknesses, that is, the orifice lengths, were found to be 0.011 ± 0.0005 in.

THEORETICAL PRINCIPLES

Torsion-Effusion Method

A diagram of the horizontal full section of an effusion cell is shown in Figure 7, in which F_1 and F_2 denote the forces exerted by a gas at pressure p as it effuses through two orifices with areas A_1 and A_2 located at distances d_1 and d_2, respectively, from the axis of rotation of the cell. If the torque D created by these forces causes the cell to rotate through an angle θ, then

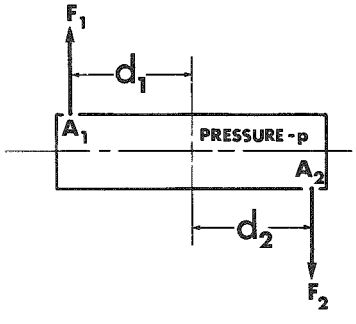

34986

Figure 7

A Horizontal Full Section of an Effusion Cell

$$D = F_1 d_1 + F_2 d_2 = \tau\theta \quad , \tag{11}$$

where τ is the torsion constant of the torsion wire.

Based on the kinetic theory of gases,[15,26,39,40] the relationship between the forces F_1 and F_2 and the pressure p is given by the equations

$$F_1 = \frac{A_1 p}{2} \text{ and } F_2 = \frac{A_2 p}{2} \tag{12}$$

when the orifices are infinitesimal in length and when the gas effuses into a vacuum. When combined with Equation (12), Equation (11) becomes

$$D = \frac{A_1 d_1 p}{2} + \frac{A_2 d_2 p}{2} = \tau\theta \quad , \tag{13}$$

which may be rewritten as

$$p = \frac{2\tau\theta}{A_1 d_1 + A_2 d_2} \quad . \tag{14}$$

The relation between deflection and pressure given in Equation (14) represents the idealized case where the orifices are of zero length. However, for orifices of finite lengths a correction must be considered. The correction factors as derived by Clausing for Knudsen effusion cells cannot be applied to torsion-effusion cells since the angular distribution of the effusing atoms must also be considered. Freeman and Searcy[16] have evaluated the correction required in terms of the ratio f of the force resulting from vapor effusing through an orifice of finite length to the force expected for the limiting case of an orifice of zero length. The correction can be approximated by

$$\frac{1}{f} = 0.0147 \left(\frac{L}{r}\right)^2 + 0.3490 \left(\frac{L}{r}\right) + 0.9982 \tag{15}$$

in the range $0 \leq L/r \leq 2.0$, where L/r is the ratio of the orifice length L to the orifice radius r.

Thus, Equation (14) must be rewritten as

$$p = \frac{2\tau\theta}{A_1 d_1 f_1 + A_2 d_2 f_2} \quad . \tag{16}$$

This is the basic equation for the determination of vapor pressure by the torsion-effusion method.

Equation (16) is valid only if free molecular flow[6,12,39] occurs, that is, if the effusion rate of the molecules is limited by collisions of the molecules against the orifice walls rather than by collisions between the molecules themselves. This condition exists when the pressure of the vapor is so low that the mean free path of the molecules, λ, is greater than the radius of the orifice. From kinetic theory,[12]

$$\lambda = \frac{1}{\sqrt{2}\pi\delta^2 n} \quad , \tag{17}$$

where δ is the molecular diameter and n is the number of molecules per unit volume. For a gas at pressure p and temperature T°K

$$n \simeq N^\circ (p/RT) \quad , \tag{18}$$

where N° is Avogadro's number and R is the ideal gas constant. The minimum mean free path calculated with Equations (17) and (18) for the present experimental conditions, where $\delta \sim 10^{-8}$ cm and $p \leq 10^{-2}$ mm Hg, give values of about one centimeter, which is approximately two orders of magnitude greater than the radius of the orifice.

Thermodynamics

A combined statement of the first and second laws of thermodynamics for a closed system doing work only against pressure is

$$dF = VdP - SdT \quad , \tag{19}$$

where F is the Gibbs free energy, V the volume, P the pressure, S the entropy, and T the absolute temperature. For one mole of an ideal gas at constant temperature, Equation (19) becomes

$$dF = RT\frac{dP}{P} = RTd\ln P \quad , \tag{20}$$

where R is the ideal gas constant. In like manner, the free energy of one mole of component A in a mixture of ideal gases at constant temperature is designated by

$$d\overline{F}_A = RTd\ \ln p_A \quad , \tag{21}$$

where $\overline{F}_A$ is the partial molar free energy and represents the change in total free energy of the mixture when one mole of component A is added to an infinite amount of the mixture, and p_A is the partial pressure of component A as defined by Dalton's law. In the case of real gases, Equations (20) and (21) become

$$dF = RTd\ \ln f \tag{22}$$

and

$$d\overline{F}_A = RTd\ \ln f_A \quad , \tag{23}$$

where f and f_A are, respectively, the fugacities of component A when pure and when in a mixture. For an ideal gas, the fugacity is equal to the pressure; but for a real gas, the fugacity and the pressure are, in general, not even proportional. As the pressure of a real gas is decreased, however, its behavior approaches that for an ideal gas so that at very low pressures

$$\lim_{P \to 0} \frac{f_A}{p_A} = 1 \quad . \tag{24}$$

For any system in equilibrium, the partial molar free energy of a given component is the same in all phases. Therefore, when the thermodynamics of the vapor in equilibrium with an alloy are evaluated, the thermodynamics of the alloy are also determined.

The thermodynamic activity of component A of an alloy a_A is defined as the ratio of its fugacity in the alloy f_A to its fugacity in its standard state f_A°; thus,

$$a_A = f_A / f_A^\circ \quad . \tag{25}$$

Ordinarily, the standard state of unit activity of a solid is chosen as the pure component under one atmosphere pressure at the temperature under consideration. In the present work, since the pressure of the vapor is quite low, it may be assumed that the metallic vapor behaves ideally; therefore, Equation (25) becomes

$$a_A = p_A / p_A^\circ \quad , \tag{26}$$

where p_A° is the pressure of the pure component A in its standard state.

Upon substituting Equation (26), Equation (21) becomes

$$d\overline{F}_A = RTd\ \ln(a_A p_A^\circ) \tag{27}$$

or

$$d\overline{F}_A = RTd\ \ln a_A + RTd\ \ln p^\circ_A \quad . \tag{28}$$

However, since p°_A is a constant at any given temperature, Equation (28) reduces to

$$d\overline{F}_A = RTd\ \ln a_A \quad . \tag{29}$$

Integration of Equation (29), at constant temperature, from the standard state to any arbitrary state gives, since $a^\circ_A = 1$,

$$\overline{F}_A - \overline{F}^\circ_A = RT\ \ln a_A = \Delta\overline{F}_A \quad , \tag{30}$$

where $\Delta\overline{F}_A$ is the relative partial molar free energy of formation of component A.

In an ideal system, the activity of component A is equal to the atomic fraction N_A, that is,

$$a_A = N_A \quad . \tag{31}$$

In a real system, the deviation of component A from ideal behavior is expressed by the ratio of the activity to the atomic fraction,

$$\gamma_A = a_A/N_A \quad , \tag{32}$$

where γ_A is defined as the activity coefficient. These last two equations are formulations of Raoult's law. The activity may, therefore, be regarded as the effective concentration of component A in the alloy.

It follows from Equation (19) that the relative partial molar entropy of formation of component A may be obtained from the temperature coefficient of $\Delta\overline{F}_A$; thus,

$$\Delta\overline{S}_A = -\left(\frac{d\Delta\overline{F}_A}{dT}\right)_P \quad . \tag{33}$$

The relative partial molar heat of formation of component A is obtained by solving the Gibbs-Helmholtz relation; thus,

$$\Delta\overline{H}_A = \Delta\overline{F}_A + T\Delta\overline{S}_A \quad . \tag{34}$$

When combined with Equation (33), Equation (34) may be rewritten as

$$\Delta\overline{H}_A = \Delta\overline{F}_A - T\left(\frac{d\Delta\overline{F}_A}{dT}\right)_P \quad . \tag{35}$$

Upon substitution of Equation (32) into Equation (30), it is seen that

$$\Delta\overline{F}_A = RT\ \ln N_A + RT\ \ln\gamma_A \quad , \tag{36}$$

where

$$RT\ \ln N_A = \Delta\overline{F}_A^{id} \tag{37}$$

and

$$RT\ \ln\gamma_A = \Delta\overline{F}_A^{ex} \quad . \tag{38}$$

Equation (37) represents the ideal part and Equation (38) the excess part of the relative partial molar free energy of formation. In a similar manner, Equation (33) becomes

$$-R\ \ln N_A = \Delta\overline{S}_A^{id} \tag{39}$$

and

$$-\left(\frac{d\Delta\overline{F}_A^{ex}}{dT}\right)_P = \Delta\overline{S}_A^{ex} \quad . \tag{40}$$

Likewise, Equation (35) becomes

$$0 = \Delta\overline{H}_A^{id} \tag{41}$$

and

$$\Delta\overline{H}_A = \Delta\overline{H}_A^{ex} \quad . \tag{42}$$

The relative partial molar thermodynamic quantities of the B component of a binary alloy are related to those of the A component by the Gibbs-Duhem equation.[41] Thus, in the case of the relative partial molar free energy,

$$N_A d\Delta\overline{F}_A + N_B d\Delta\overline{F}_B = 0 \tag{43}$$

or, in terms of activities,

$$N_A d\ \ln a_A + N_B d\ \ln a_B = 0 \quad . \tag{44}$$

Integration of Equation (44) gives

$$\ln a_B = \int_{N_B = 1}^{N_B = N_B} -\frac{N_A}{N_B}\, d\ \ln a_A \quad . \tag{45}$$

If a_A is known for all values of N_B from 1 to 0, Equation (45) may be used to determine the activity of component B. Unfortunately, however, the integrand approaches infinity as $N_B \rightarrow 0$ and $\ln a_A$ approaches minus infinity as $N_B \rightarrow 1$, which makes the integration difficult and imprecise.

Darken and Gurry,[42] seeking to alleviate this mathematical difficulty, have introduced a function designated α, which is defined for binary alloys as

$$\alpha_A = \frac{\ln \gamma_A}{N_B^2} \quad , \tag{46}$$

that is finite at all concentrations. Differentiation of Equation (46) gives

$$d \ln \gamma_A = 2\alpha_A N_B dN_B + N_B^2 d\alpha_A \quad , \tag{47}$$

which, when substituted into Equation (45) written in terms of the activity coefficient, is

$$\ln \gamma_B = - \int_{N_B = 1}^{N_B = N_B} 2\alpha_A N_A dN_B - \int_{N_B = 1}^{N_B = N_B} N_A N_B d\alpha_A \tag{48}$$

or, when partially solved,

$$\ln \gamma_B = - \alpha_A N_B N_B - \int_{N_B = 1}^{N_B = N_B} \alpha_A dN_B \quad . \tag{49}$$

Graphical integration of Equation (49) is straightforward.

In view of the difficulties in solving the Gibbs-Duhem equation, it is generally considered more accurate to solve only for $\Delta \overline{F}_B$. The quantities $\Delta \overline{S}_B$ and $\Delta \overline{H}_B$ can then be calculated from equations similar to Equations (33) and (34). In like manner, $\Delta \overline{F}_B^{ex}$ and $\Delta \overline{S}_B^{ex}$ may be calculated from equations similar to Equations (38) and (40).

The integral thermodynamic functions of a binary alloy are related to the partial functions as follows:

$$\Delta F = N_A \overline{F}_A + N_B \Delta \overline{F}_B \quad , \tag{50}$$

$$\Delta F^{id} = N_A \Delta \overline{F}_A^{id} + N_B \Delta \overline{F}_B^{id} \quad , \tag{51}$$

$$\Delta F^{ex} = N_A \Delta \overline{F}_A^{ex} + N_B \Delta \overline{F}_B^{ex} \quad , \tag{52}$$

$$\Delta S = N_A \Delta \bar{S}_A + N_B \Delta \bar{S}_B \quad , \tag{53}$$

$$\Delta S^{id} = N_A \Delta \bar{S}_A^{id} + N_B \Delta \bar{S}_B^{id} \quad , \tag{54}$$

$$\Delta S^{ex} = N_A \Delta \bar{S}_A^{ex} + N_B \Delta \bar{S}_B^{ex} \quad , \tag{55}$$

$$\Delta H = N_A \Delta \bar{H}_A + N_B \Delta \bar{H}_B = \Delta H^{ex} \quad , \tag{56}$$

and

$$\Delta H^{id} = 0 \quad . \tag{57}$$

RESULTS

Vapor Pressures

The Clausius-Clapeyron equation,

$$\frac{d\ln p}{dT} = \frac{\Delta H_s}{RT^2} \quad , \tag{58}$$

in which ΔH_s is the latent heat of sublimation, defines the temperature dependence of the vapor pressure p of a solid if the vapor behaves ideally and if the specific volume of the vapor greatly exceeds that of the solid.

If ΔH_s is assumed to be a constant, integration of Equation (58) gives

$$\ln p = \frac{-\Delta H_s}{RT} + C \quad , \tag{59}$$

where C is an integration constant. Thus, when both of the above conditions are fulfilled over the experimental temperature range, a plot of the natural logarithm of the vapor pressures versus the reciprocal of the absolute temperatures should be linear. In these experiments, however, an inaccuracy in the determination of the zero point of the suspension resulted in the experimental data that deviated from a straight line. A typical experimental curve is shown in Figure 8. It is believed that the origin of this uncertainty may be associated with an anelastic relaxation of the torsion wire at the initial onset of rotation.

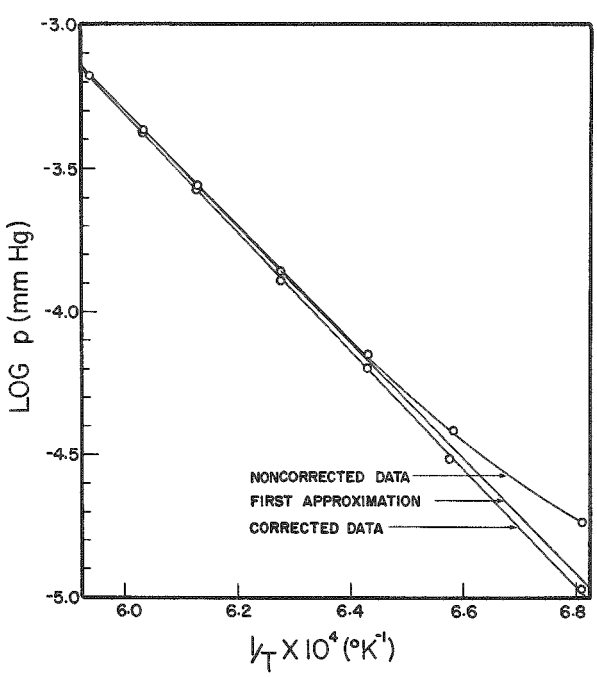

34981

Figure 8. Plot of the Noncorrected and the Corrected Data for the $Fe_{0.4}$-$V_{0.6}$ Alloy.

The inaccuracy in the zero point represented an error of about 10 per cent for the two or three smallest rotations and of about 0.1 per cent for most of the remaining rotations. The data were corrected by a method of successive approximations. The method, as shown in Figure 8, consisted of four steps: (1) A straight line was drawn through the three or four points of

greatest deflection. (2) A corrected zero point was determined that would correct one of the remaining data points to this line. (3) The corrected zero point was then used to recalculate all of the remaining data points. (4) The best-fit straight line through all of the corrected data points was found by the method of least squares. In most cases, one such operation was sufficient to correct the data to a linear curve, but in a few cases, two such operations were necessary. The noncorrected and corrected data are given in Tables II through XIII. The corrected vapor pressure curves are shown in Figure 9 for pure iron and for iron measured over various vanadium-iron alloys in Figure 10. The equations for these curves are given in Table XIV.

Table II

VAPOR PRESSURES OF IRON

Cell Ta 3, Torsion Constant = 2.259 dyne-cm/rad

Temp (°K)	Deflection (in.)	Pressure p (mm Hg x 10^5)	-log p	Pressure p* (mm Hg x 10^5)	-log p*	$\frac{1}{T} \times 10^4$
1452	0.20	2.984	4.525	4.328	4.364	6.887
1473	0.37	5.517	4.258	6.839	4.165	6.789
1492	0.61	9.091	4.041	10.43	3.982	6.702
1512	0.99	14.74	3.832	16.09	3.793	6.614
1533	1.59	23.67	3.626	25.01	3.602	6.523
1556	2.56	38.09	3.419	39.42	3.404	6.427
1574	3.72	55.30	3.257	56.64	3.247	6.353
1596	5.65	83.93	3.076	85.28	3.069	6.266
1615	8.22	122.0	2.914	123.4	2.909	6.192
1632	11.27	167.3	2.777	168.6	2.773	6.127
1657	17.44	258.6	2.587	260.0	2.585	6.035
1677	24.82	367.9	2.434	369.3	2.433	5.963

*Corrected values.

Table III

VAPOR PRESSURES OF IRON

Cell Ta 5, Torsion Constant = 0.7497 dyne-cm/rad

Temp (°K)	Deflection (in.)	Pressure p (mm Hg x 10^5)	-log p	Pressure p* (mm Hg x 10^5)	-log p*	$\frac{1}{T} \times 10^4$
1451	1.06	3.213	4.493	4.169	4.380	6.892
1471	1.81	5.484	4.261	6.454	4.190	6.798
1493	3.21	9.721	4.012	10.69	3.971	6.698
1509	4.62	13.98	3.854	14.95	3.825	6.627
1530	7.34	22.20	3.654	23.17	3.635	6.536
1548	10.96	33.13	3.480	34.10	3.467	6.460
1566	15.83	47.82	3.320	48.79	3.312	6.386
1585	22.19	66.97	3.174	67.96	3.168	6.309

*Corrected values.

Table IV

VAPOR PRESSURES OF IRON

Cell Ta 5, Torsion Constant = 0.7358 dyne-cm/rad

Temp (°K)	Deflection (in.)	Pressure p (mm Hg x 10^5)	-log p	Pressure p* (mm Hg x 10^5)	-log p*	$\frac{1}{T} \times 10^4$
1468	2.21	6.533	4.185	none required	none required	6.812
1509	5.32	15.71	3.804	"	"	6.627
1549	12.03	35.50	3.450	"	"	6.456
1579	21.71	63.98	3.194	"	"	6.333
1614	41.39	121.9	2.914	"	"	6.196
1635	60.02	176.6	2.753	"	"	6.116
1647	74.51	219.2	2.659	"	"	6.072
1660	93.47	274.8	2.561	"	"	6.024

*Corrected values.

Table V

VAPOR PRESSURES OF IRON OVER VANADIUM-IRON ALLOYS

Cell Ta 6, Torsion Constant = 0.7338 dyne-cm/rad

Temp (°K)	Deflection (in.)	Pressure p (mm Hg x 10^5)	-log p	Pressure p* (mm Hg x 10^5)	-log p*	$\frac{1}{T} \times 10^4$
1467	1.60	7.365	4.133	5.445	4.264	6.817
1507	3.39	15.59	3.807	13.65	3.865	6.636
1547	7.17	32.93	3.482	31.00	3.509	6.464
1582	13.76	63.13	3.200	61.20	3.213	6.321
1616	25.05	114.8	2.940	112.9	2.957	6.188
1635	35.25	161.4	2.792	159.5	2.797	6.116
1659	53.07	242.9	2.615	241.0	2.618	6.028
1672	64.88	296.8	2.528	294.8	2.530	5.981

*Corrected values.

Table VI

VAPOR PRESSURES OF IRON OVER VANADIUM-IRON ALLOYS

Cell Ta 7, Torsion Constant = 0.7454 dyne-cm/rad

Temp (°K)	Deflection (in.)	Pressure p (mm Hg x 10^5)	-log p	Pressure p* (mm Hg x 10^5)	-log p*	$\frac{1}{T} \times 10^4$
1472	1.71	7.966	4.099	5.297	4.276	6.793
1507	2.97	13.82	3.859	11.17	3.952	6.636
1547	5.78	26.87	3.571	24.22	3.616	6.464
1581	10.45	48.54	3.314	45.89	3.338	6.325
1606	16.06	74.53	3.128	71.89	3.143	6.227
1632	25.40	117.8	2.929	115.1	2.939	6.127
1656	37.40	173.3	2.761	170.6	2.768	6.039
1666	44.89	207.9	2.682	205.3	2.688	6.002

*Corrected values.

Table VII

VAPOR PRESSURES OF IRON OVER VANADIUM-IRON ALLOYS

Cell Ta 8, Torsion Constant = 0.7429 dyne-cm/rad

Temp (°K)	Deflection (in.)	Pressure p (mm Hg x 10^5)	-log p	Pressure p* (mm Hg x 10^5)	-log p*	$\frac{1}{T} \times 10^4$
1468	0.72	3.337	4.477	3.648	4.438	6.812
1506	1.69	7.823	4.107	8.146	4.089	6.640
1548	3.95	18.26	3.738	18.59	3.731	6.460
1580	7.23	33.39	3.476	33.72	3.472	6.329
1604	11.18	51.60	3.287	51.90	3.285	6.234
1629	17.53	80.86	3.092	81.16	3.091	6.139

*Corrected values.

Table VIII

VAPOR PRESSURES OF IRON OVER VANADIUM-IRON ALLOYS

Cell Ta 9. Torsion Constant = 0.7454 dyne-cm/rad

Temp (°K)	Deflection (in.)	Pressure p (mm Hg x 10^5)	-log p	Pressure p* (mm Hg x 10^5)	-log p*	$\frac{1}{T} \times 10^4$
1454	0.44	2.051	4.688	2.123	4.673	6.878
1508	1.36	6.327	4.199	6.420	4.192	6.631
1547	2.93	13.61	3.866	13.71	3.863	6.464
1577	5.29	25.56	3.610	24.65	3.608	6.341
1606	8.86	41.10	3.386	41.19	3.385	6.227
1630	13.51	62.62	3.203	62.71	3.203	6.135
1655	20.77	96.16	3.017	96.31	3.016	6.042
1668	25.76	119.2	2.924	119.3	2.923	5.995

*Corrected values.

Table IX

VAPOR PRESSURES OF IRON OVER VANADIUM-IRON ALLOYS

Cell Ta 10, Torsion Constant = 0.7423 dyne-cm/rad

Temp (°K)	Deflection (in.)	Pressure p (mm Hg x 10^5)	-log p	Pressure p* (mm Hg x 10^5)	-log p*	$\frac{1}{T} \times 10^4$
1469	0.42	1.979	4.704	1.762	4.754	6.807
1506	0.87	4.094	4.388	3.858	4.414	6.640
1551	2.02	9.496	4.022	9.256	4.034	6.447
1585	3.77	17.70	3.752	17.46	3.758	6.309
1607	5.70	26.73	3.573	26.51	3.577	6.223
1632	8.67	40.64	3.391	40.41	3.394	6.127
1656	13.27	62.15	3.207	61.92	3.208	6.039
1669	16.47	77.11	3.113	76.88	3.114	5.992

*Corrected values.

Table X

VAPOR PRESSURES OF IRON OVER VANADIUM-IRON ALLOYS

Cell Ta 11, Torsion Constant = 0.7392 dyne-cm/rad

Temp (°K)	Deflection (in.)	Pressure p (mm Hg x 10^5)	-log p	Pressure p* (mm Hg x 10^5)	-log p*	$\frac{1}{T} \times 10^4$
1468	0.40	1.826	4.738	1.030	4.987	6.812
1519	0.84	3.830	4.417	3.054	4.515	6.583
1555	1.56	7.105	4.148	6.330	4.199	6.431
1593	3.02	13.73	3.862	12.96	3.887	6.277
1631	6.06	27.53	3.560	26.75	3.573	6.131
1657	9.48	43.03	3.366	42.26	3.374	6.035
1683	14.71	66.72	3.176	65.95	3.181	5.942
1704	21.17	95.93	3.018	95.18	3.021	5.869

*Corrected values.

Table XI

VAPOR PRESSURES OF IRON OVER VANADIUM-IRON ALLOYS

Cell Ta 12, Torsion Constant = 0.7392 dyne-cm/rad

Temp (°K)	Deflection (in.)	Pressure p (mm Hg x 10^5)	-log p	Pressure p* (mm Hg x 10^5)	-log p*	$\frac{1}{T} \times 10^4$
1474	0.28	1.061	4.974	0.6622	5.179	6.784
1526	0.66	2.498	4.602	2.081	4.682	6.553
1577	1.62	6.120	4.213	5.328	4.273	6.341
1632	4.34	16.37	3.786	15.95	3.797	6.127
1659	7.05	26.57	3.576	26.15	3.583	6.028
1681	10.38	39.09	3.408	38.68	3.413	5.949
1706	15.81	59.49	3.226	59.07	3.229	5.862
1727	22.22	83.56	3.078	83.18	3.080	5.790
1756	34.88	131.0	2.883	130.7	2.884	5.695

*Corrected values.

Table XII

VAPOR PRESSURES OF IRON OVER VANADIUM-IRON ALLOYS

Cell Ta 13, Torsion Constant = 0.7431 dyne-cm/rad

Temp (°K)	Deflection (in.)	Pressure p (mm Hg x 10^5)	-log p	Pressure p* (mm Hg x 10^5)	-log p*	$\frac{1}{T} \times 10^4$
1527	0.44	2.018	4.695	1.076	4.968	6.549
1578	0.88	4.031	4.395	3.068	4.513	6.337
1631	2.05	9.376	4.028	8.416	4.075	6.131
1657	3.15	14.39	3.842	13.44	3.872	6.035
1681	4.64	21.19	3.674	20.22	3.694	5.949
1702	6.58	30.02	3.523	29.07	3.537	5.875
1728	10.13	46.19	3.335	45.23	3.345	5.787
1574	15.20	69.25	3.160	68.29	3.166	5.701
1767	18.67	84.98	3.071	84.08	3.075	5.659

*Corrected values.

Table XIII

VAPOR PRESSURES OF IRON OVER VANADIUM-IRON ALLOYS

Cell Ta 14, Torsion Constant = 0.7431 dyne-cm/rad

Temp (°K)	Deflection (in.)	Pressure p (mm Hg x 10^5)	-log p	Pressure p* (mm Hg x 10^5)	-log p*	$\frac{1}{T} \times 10^4$
1631	0.38	1.738	4.760	0.957	5.019	6.131
1657	0.52	2.375	4.624	1.599	4.796	6.035
1679	0.71	3.241	4.489	2.420	4.616	5.956
1703	1.00	4.562	4.341	3.786	4.422	5.872
1727	1.48	6.747	4.171	5.971	4.224	5.790
1753	2.25	10.25	3.989	9.473	4.024	5.705
1773	3.14	14.30	3.845	13.52	3.869	5.640
1800	4.80	21.83	3.661	21.06	3.677	5.556

*Corrected values.

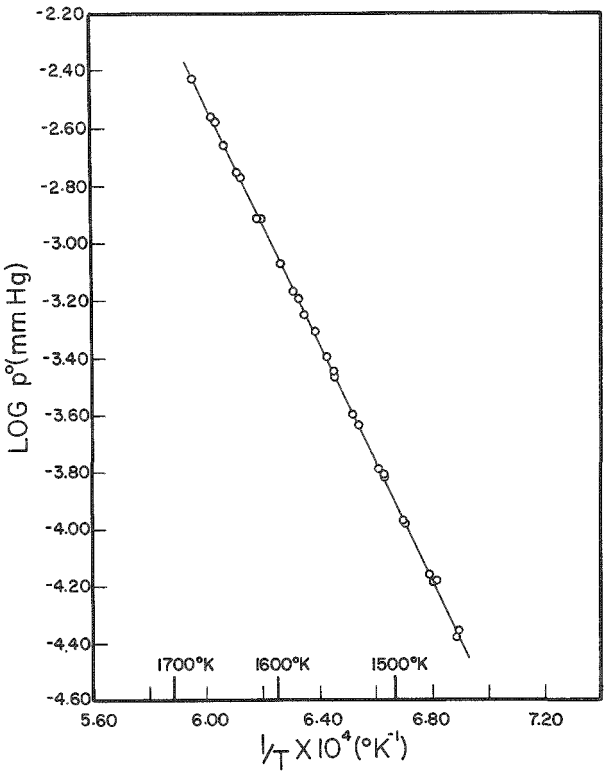

34985

Figure 9. The Vapor Pressure of Iron

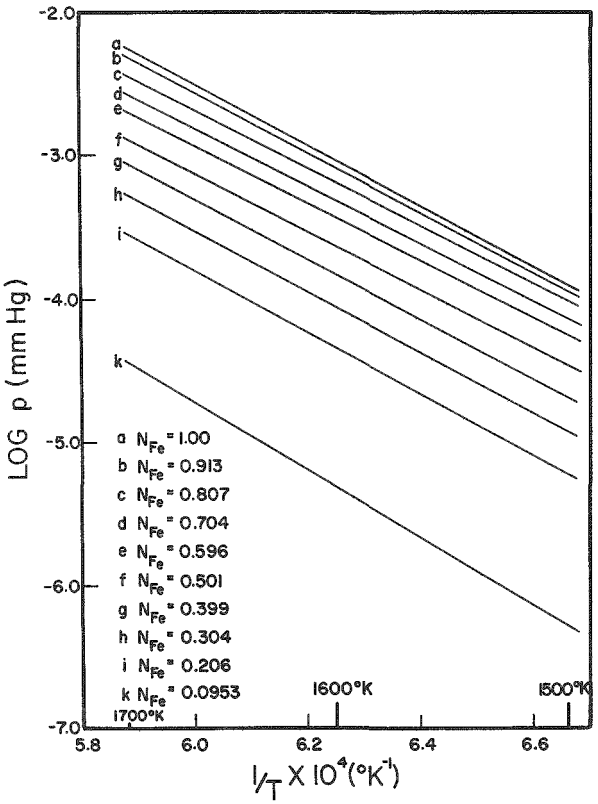

34993

Figure 10. Vapor Pressure Curves of Iron over Vanadium-Iron Alloys.

Table XIV

EQUATIONS OF THE CORRECTED VAPOR PRESSURE CURVES IN THE FORM, $\log_{mm\ Hg} P = (m/T) + b$

N_{Fe}	m	b	N_{Fe}	m	b
1.00*	-20908	10.036	0.501	-20087	8.920
0.913	-20751	9.888	0.399	-20774	9.161
0.807	-20096	9.373	0.304	-21070	9.118
0.704	-19984	9.178	0.206	-21238	8.943
0.596	-19810	8.952	0.095	-23411	9.331

*Least-squares fit to data contained in Tables II, III, and IV.

It was noted earlier that the assumption that the equilibrium pressure within the cell was not disturbed by the orifice openings was subject to some limitations. In an effort to confirm the conclusions made by Speiser,[8] Cells Ta3 and Ta5 were constructed with orifices that differed

in area by a factor of $1\frac{1}{2}$ from one cell to the other. If equilibrium was not attained within the cell, the observed vapor pressures would be dependent upon the size of the orifice. The two sets of vapor pressure data obtained from the use of these cells, as seen in Tables II and III, were in agreement to well within experimental scatter, indicating that the above assumption was legitimate for the present experimental conditions.

The main errors in the present work are likely to be associated with the determination of the cell temperature and with the measurement of the zero point. Errors in the measurement of the cell dimensions are at most ± 0.1 per cent and represented an error of about ± 0.3 per cent in the vapor pressure. Any errors in the evaluation of the torsion constant are considered to be negligible. Based on repetitive experimental runs with the same cells (see for example Tables III and IV), a reasonable estimate of the experimental precision of the vapor pressure values is ± 2 per cent.

Thermodynamics

Since the crystal structure of the alloys in the temperature range investigated is body-centered cubic (bcc), pure bcc alpha iron at 1600°K was taken as the reference state for all of the thermodynamic data presented in this report. As the allotrope of iron at 1600°K is face-centered cubic (fcc), it was necessary to consider the magnitude of the correction required to convert the free energies of fcc gamma iron to those of alpha iron. Values of the free energy of transformation of gamma iron to alpha iron(43,44) show that the difference in free energy between the two allotropes at 1600°K is about 9 cal/gm-atom. However, the free energy of sublimation ΔF° of gamma iron at unit pressure, which is related to the vapor pressure p° at any temperature by the expression.

$$\Delta F^\circ = -RT \ln p^\circ \quad , \tag{60}$$

was found to be approximately 43290 cal/gm-atom at 1600°K. Therefore, the conversion of standard states represents a correction to the free energy of only about 0.02 per cent at 1600°K. As a correction of this size falls well within the limit of experimental error, the free energies of formation were computed on the basis of the vapor pressures of gamma iron rather than on the basis of the vapor pressures of hypothetical alpha iron.

The activities of iron were calculated at 1500, 1600, and 1700°K from the vapor pressure data and were curve-fitted by the least-squares method. The activities of iron at 1600°K and the activities of vanadium, as determined by the Gibbs-Duhen equation, are shown in Figure 11 and are tabulated in Table XV.

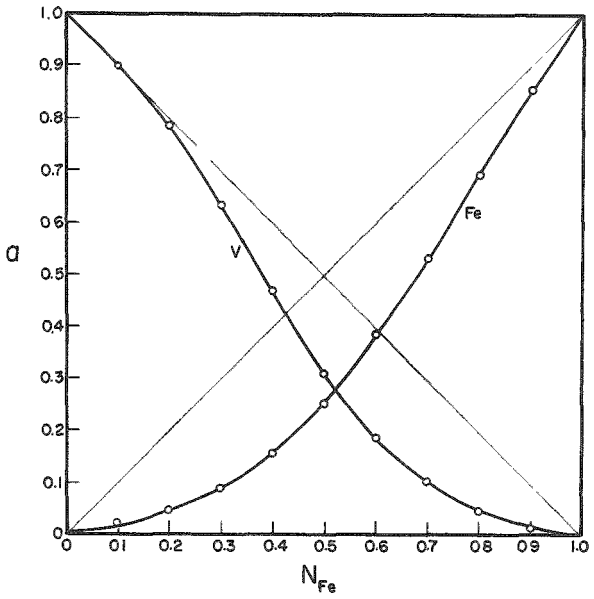

34996

Figure 11

Activities of Iron and Vanadium in the Vanadium-Iron Alloy System at 1600°K

Table XV

ACTIVITIES OF IRON AND VANADIUM IN THE VANADIUM-IRON ALLOY SYSTEM AT 1600°K

N_{Fe}	a_{Fe}	a_V	N_{Fe}	a_{Fe}	a_V
1.0	1.0000	0.0000	0.4	0.155	0.4698
0.9	0.856	0.0138	0.3	0.0870	0.6335
0.8	0.695	0.0466	0.2	0.0460	0.7872
0.7	0.534	0.1032	0.1	0.0207	0.900
0.6	0.387	0.1884	0.0	0.0000	1.0000
0.5	0.256	0.3120			

The partial free energies of formation of iron and vanadium at 1600°K are shown in Figure 12 and are tabulated in Table XVI. The partial entropies of formation, which were calculated by means of the relation

$$\Delta\bar{S}_{1600} = -\frac{\Delta\bar{F}_{1700} - \Delta\bar{F}_{1500}}{200} \qquad (61)$$

are plotted in Figure 13 and are listed in Table XVI. The partial heats of formation are shown in Figure 14 and are given in Table XVI. The integral free energies, entropies, and heats are plotted in Figure 15 and are recorded in Table XVII. The partial excess free energies and partial excess entropies are given in Figures 16 and 17, respectively, and are listed in Table XVIII. Integral values of the excess free energy, excess entropy, and heats of formation are shown in Figure 18 and are tabulated in Table XIX.

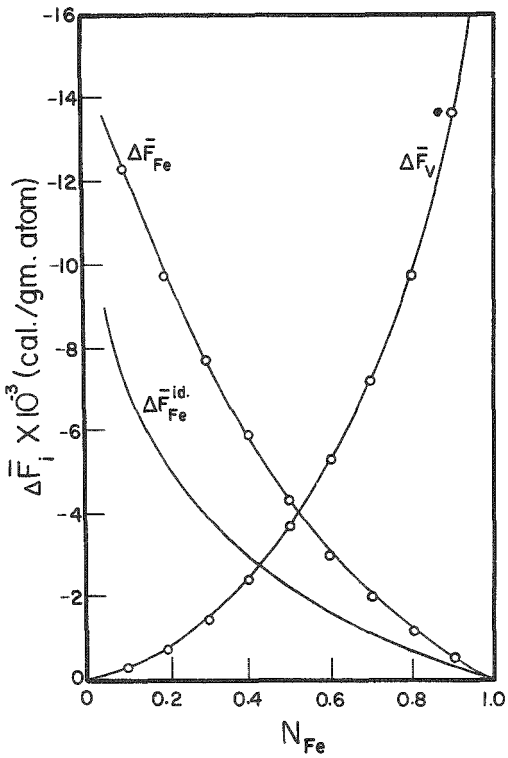

34988

Figure 12

Partial Free Energies of Formation in the Vanadium-Iron Alloy System at 1600°K

Table XVI

PARTIAL FREE ENERGIES, ENTROPIES, AND HEATS OF FORMATION IN THE VANADIUM-IRON ALLOY SYSTEM AT 1600°K

N_{Fe}	$\Delta\bar{F}_{Fe}$, cal/gm-atom	$\Delta\bar{F}_{V}$, cal/gm-atom	$\Delta\bar{S}_{Fe}$, cal/(gm-atom)(deg)	$\Delta\bar{S}_{V}$, cal/(gm-atom)(deg)	$\Delta\bar{H}_{Fe}$, cal/gm-atom	$\Delta\bar{H}_{V}$, cal/gm-atom
1.0	0		0		0	
0.9	-494	-13616	1.46	11.26	1842	4400
0.8	-1157	-9747	2.54	4.82	2907	-2035
0.7	-1995	-7226	3.32	2.36	3317	-3450
0.6	-3018	-5313	3.82	1.46	3094	-2977
0.5	-4332	-3702	4.06	0.985	2164	-2126
0.4	-5927	-2400	4.12	1.09	665	-656
0.3	-7763	-1449	4.04	1.13	-1299	359
0.2	-9788	-761	4.67	0.935	-2316	735
0.1	-12327	-335	7.55	0.220	247	17
0.0		0		0		0

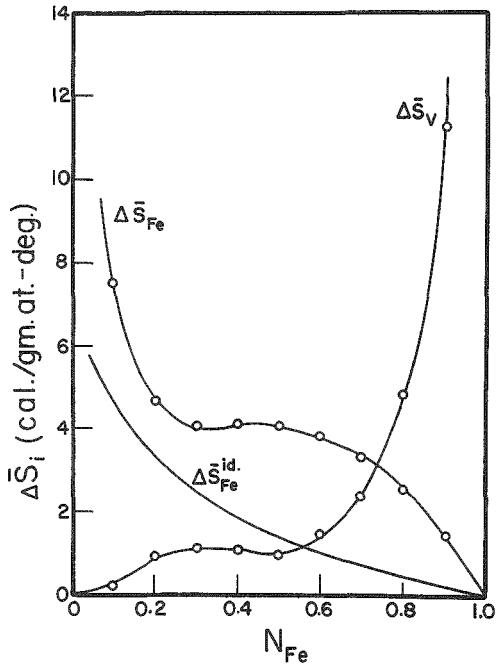

Figure 13

Partial Entropies of Formation in the Vanadium-Iron Alloy System at 1600°K

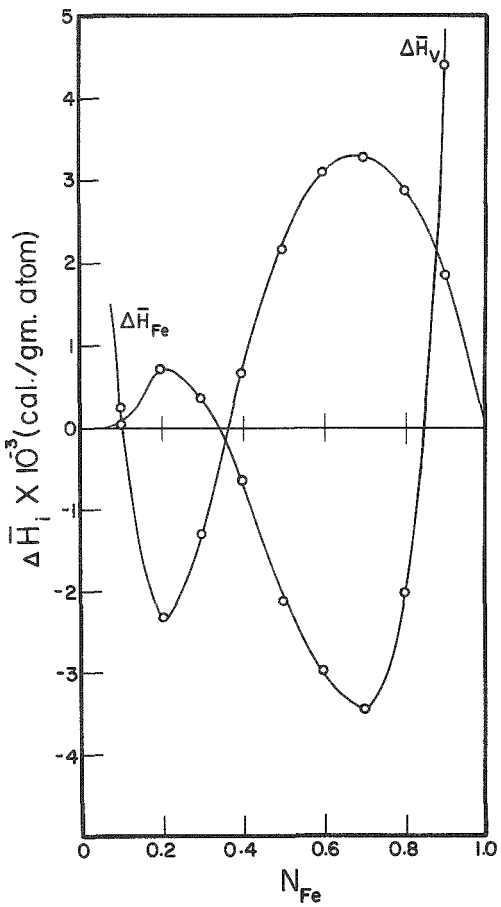

34984

Figure 14. Partial Heats of Formation in the Vanadium-Iron Alloy System at 1600°K.

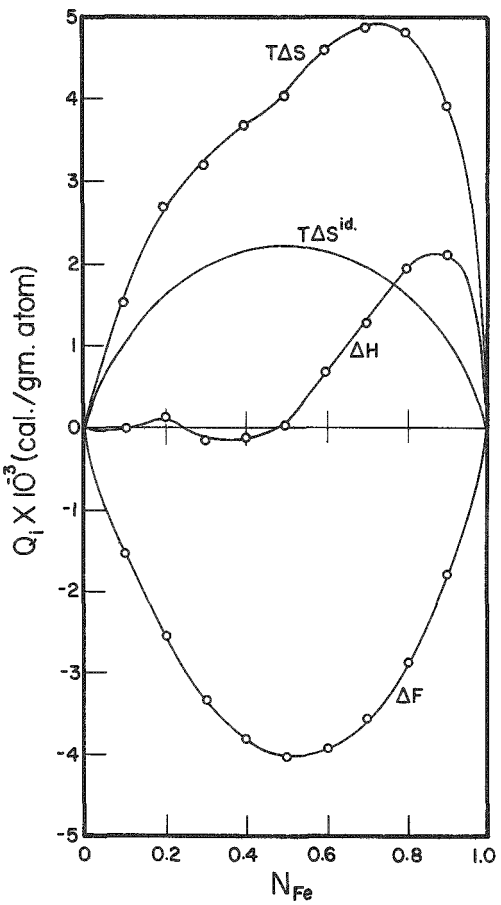

34992

Figure 15. Integral Free Energies, Entropies, and Heats of Formation in the Vanadium-Iron Alloy System at 1600°K.

Table XVII

INTEGRAL FREE ENERGIES, ENTROPIES, AND HEATS OF FORMATION IN THE VANADIUM-IRON ALLOY SYSTEM AT 1600°K

N_{Fe}	ΔF, cal/gm-atom	$T\Delta S$ cal/gm-atom	ΔH, cal/gm-atom	N_{Fe}	ΔF, cal/gm-atom	$T\Delta S$, cal/gm-atom	ΔH, cal/gm-atom
1.0	0	0	0	0.4	-3811	3680	-131
0.9	-1806	3904	2098	0.3	-3343	3200	-143
0.8	-2875	4800	1925	0.2	-2566	2688	122
0.7	-3564	4848	1284	0.1	-1534	1525	-9
0.6	-3936	4608	672	0.0	0	0	0
0.5	-4017	4032	15				

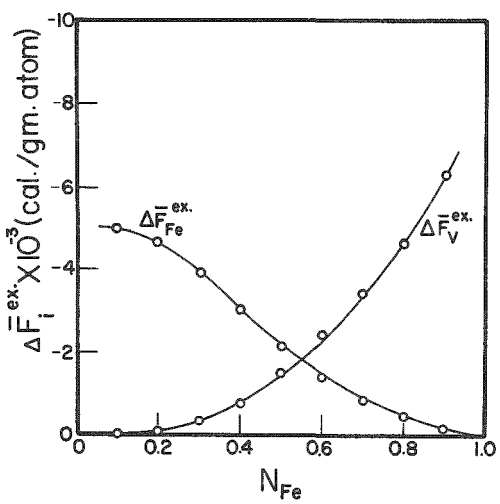

34990

Figure 16. Partial Excess Free Energies of Formation in the Vanadium-Iron Alloy System at 1600°K.

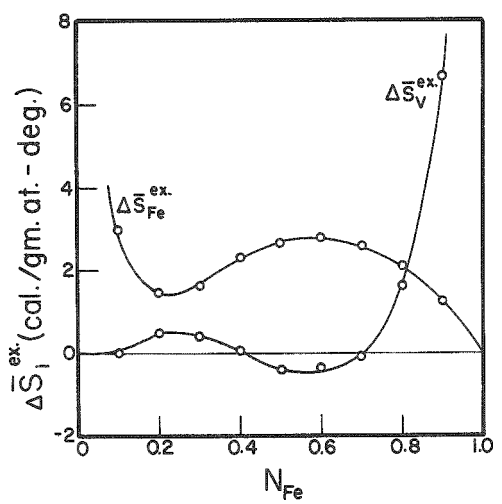

34987

Figure 17. Partial Excess Entropies of Formation in the Vanadium-Iron Alloy System at 1600°K.

Table XVIII

PARTIAL EXCESS FREE ENERGIES AND ENTROPIES OF FORMATION IN THE VANADIUM-IRON ALLOY SYSTEM AT 1600°K

N_{Fe}	$\Delta\bar{F}_{Fe}^{ex}$, cal/gm-atom	$\Delta\bar{F}_V^{ex}$, cal/gm-atom	$\Delta\bar{S}_{Fe}^{ex}$, cal/(gm-atom)(deg)	$\Delta\bar{S}_V^{ex}$, cal/(gm-atom)(deg)
1.0	0		0	
0.9	-159	-6296	1.25	6.68
0.8	-448	-4630	2.10	1.62
0.7	-861	-3398	2.61	-0.040
0.6	-1394	-2400	2.80	-0.360
0.5	-2129	-1499	2.68	-0.395
0.4	-3014	-766	2.30	0.070
0.3	-3935	-315	1.64	0.420
0.2	-4671	-52	1.47	0.490
0.1	-5007	0	2.97	0.01
0.0		0		0

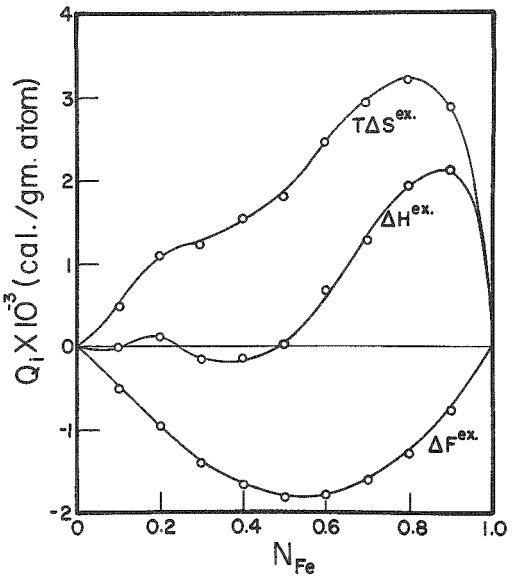

34983

Figure 18

Integral Excess Free Energies, Entropies, and Heats of Formation in the Vanadium-Iron Alloy System at 1600°K.

Table XIX

INTEGRAL EXCESS FREE ENERGIES AND ENTROPIES OF FORMATION IN THE VANADIUM-IRON ALLOY SYSTEM AT 1600°K

N_{Fe}	ΔF^{ex}, $\left(\frac{cal}{gm\text{-}atom}\right)$	$T\Delta S^{ex}$, $\left(\frac{cal}{gm\text{-}atom}\right)$	N_{Fe}	ΔF^{ex}, $\left(\frac{cal}{gm\text{-}atom}\right)$	$T\Delta S^{ex}$, $\left(\frac{cal}{gm\text{-}atom}\right)$
1.0	0	0	0.4	-1671	1536
0.9	-772	2880	0.3	-1401	1248
0.8	-1284	3200	0.2	-975	1096
0.7	-1622	2896	0.1	-500	493
0.6	-1796	2464	0.0	0	0
0.5	-1814	1824			

The estimated average precision for the activities and for the corresponding partial free energies is ±4 per cent. However, because the activity values are obtained from the relation

$$\log a = \log p - \log p^\circ \quad ,$$

small errors in p or p° can lead to considerable uncertainty in a, especially when p and p° are approximately equal. It is difficult to assess the errors in the integral entropies or enthalpies as slight deviations in the relative slopes of the vapor pressure curves can result in very large errors in these thermodynamic quantities. An estimate of these errors is ±0.5 cal/(gm-atom)(deg) for the integral entropies and ±500 cal/gm-atom for the integral enthalpies.

DISCUSSION

Vapor Pressure of Iron

The vapor pressure of solid iron has been reported by a number of investigators.[26,45-55] A graphical comparison of the results of these studies with a plot of the vapor pressure equation derived in the present work is made in Figure 19.

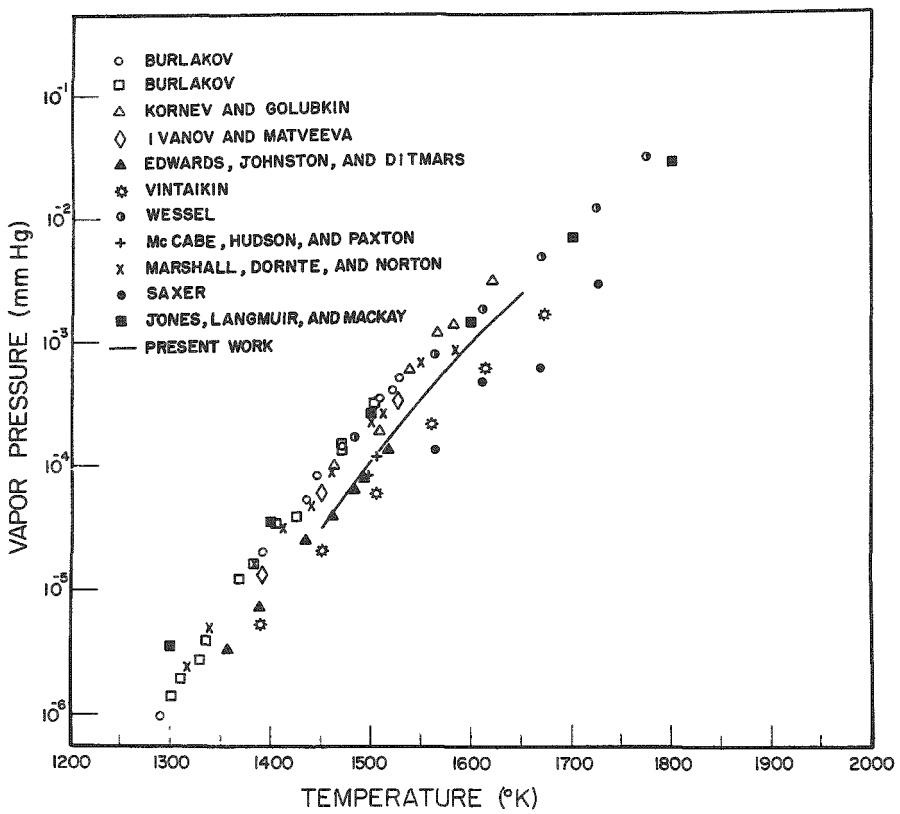

Figure 19. Vapor Pressure of Solid Iron[56]

The first significant determination of the vapor pressure of iron was made by Langmuir et al.,[45] who measured the rate of evaporation of an iron filament of unreported purity in the temperature range from 1270 to 1580°K. The standard latent heat of sublimation at 298.15°K, ΔH°_{298}, calculated from these data was 96715 ± 250 cal/gm-atom.[57] A decade later Marshall et al.,[46] in an attempt to improve the Langmuir method, replaced the filament by a high-purity iron ring. Temperatures in the range from 1317 to 1579°K were determined by an optical pyrometer. The average value of ΔH°_{298} was found to be 97290 ± 400 cal/gm-atom.[57] Edwards and coworkers[47] further refined the Langmuir method and determined the vapor pressure of vacuum cast, 99.97 per cent pure iron between 1356 and 1519°K. The temperature was measured with an optical pyrometer.

On the basis of these data, the standard heat of sublimation has been taken as 99810 ± 150 cal/gm-atom.[57] Burlakov,[48] using the Langmuir method, found different values for the vapor pressure of 99.89 per cent pure iron depending on whether the sample was condensed from the vapor or vacuum cast. He suggested that the difference may be the result of a preferred texture in the condensed metal surface. Kornev and Golubkin[49] determined the vapor pressure of 99.85 per cent pure gamma iron between 1464 and 1623°K by the Langmuir method by counting the activity of Fe^{56} deposited on collector plates.

The Knudsen method was employed by Vintaikin,[51] who used Fe^{59} as a tracer element to determine the vapor pressure of electrolytic iron between 1430 and 1670°K. Computed from these data, the value of ΔH°_{298} was found to be 98780 cal/gm-atom.[57] Ivanov et al.[52] determined the vapor pressure of annealed technical iron by means of the Knudsen isotope-exchange method[58] with Fe^{59} as the tracer element. Recently, Saxer[54] determined the vapor pressure of iron between 1562 and 1724°K with an induction-heated alumina Knudsen cell and obtained a mean value of ΔH°_{298} of 99053 cal/gm-atom.

Wessel[26] measured the vapor pressure of iron by the torsion-effusion method in which cells of quartz, alumina, and graphite were suspended from a tungsten wire into a graphite sheath furnace. An optical pyrometer was used to measure the temperature of the cell. No correction was made for the finite thickness of the cell orifices.

The reliability of the vapor pressure data for solid iron that were accumulated in the present work is indicated by the temperature independence of the calculated values of ΔH°_{298}. The difficulty in obtaining an accurate temperature coefficient of the vapor pressure often precludes a reliable determination of the heat of sublimation by means of Equation (59). The third-law test method, on the other hand, minimizes these temperature dependent errors and gives reasonably good results.[59] Hence, values of ΔH°_{298} were evaluated from the experimental data by means of the third-law test equation

$$\Delta H^\circ_{298} = -T\left[R \ln p^\circ + \left(\frac{\Delta F^\circ - \Delta H^\circ_{298}}{T}\right)\right] , \qquad (62)$$

where the parenthetical term is the difference between the free energy functions of iron vapor and of solid iron at the temperature under consideration.[59] The computed values are listed in Table XX. The mean value of ΔH°_{298}, 99000 ± 150 cal/gm-atom, agrees favorably with the value of 98600 ± 1500 cal/gm-atom compiled by Hultgren.[57]

Table XX

HEAT OF SUBLIMATION OF IRON AT 298.16°K

Table	Temperature (°K)	ΔH°_{298} $\left(\frac{\text{cal}}{\text{gm-atom}}\right)$	Table	Temperature (°K)	ΔH°_{298} $\left(\frac{\text{cal}}{\text{gm-atom}}\right)$
II	1452	99079	III	1493	99072
"	1473	99111	"	1509	99081
"	1492	99081	"	1530	99069
"	1512	99034	"	1548	98982
"	1533	99016	"	1566	98976
"	1556	99030	"	1585	99085
"	1574	98998	IV	1458	98924
"	1596	99017	"	1509	98936
"	1615	98949	"	1549	98925
"	1632	98927	"	1579	98913
"	1657	98951	"	1614	98925
"	1677	98913	"	1635	98960
III	1451	99105	"	1647	98945
"	1471	99145	"	1660	98931

Thermodynamics

In the past, various models have been proposed to interpret the thermodynamic properties of metallic solid solutions in terms of those of pure components.[60,61] However, sufficient thermodynamic data on metal solutions now exist to show clearly that it is necessary to consider, in addition to the configurational contributions that are developed by these theories, the nature of the electronic and magnetic interactions between the atoms.[61,62] Hence, only an empirical interpretation of the results of the present work has been attempted.

As may be seen in Figure 11, the experimentally determined activities of iron exhibit negative deviations from ideality. The calculated activities of vanadium are also characterized by negative deviations in the iron-rich alloys, but they approach ideality in the vanadium-rich alloys. With increasing temperature, the deviations from ideality increase for the solvent atoms and decrease for the solute atoms. Negative deviations from ideality suggest that the attractive forces, which exist between atoms of unlike kind, are predominant.

The most interesting thermodynamic properties, insofar as alloy chemistry is concerned, are the excess quantities, which depict deviations from ideal behavior. The integral values of the excess quantities found in this research are shown in Figure 18. Whereas the plot of ΔF^{ex} is slightly asymmetrical with a single minimum, the plots of both ΔS^{ex} and ΔH^{ex} are

quite asymmetrical and appear to have two maxima. As a result, ΔS^{ex} and ΔH^{ex} would seem to be a composite of a number of contributions.

The minimum in the excess free energies occurs at approximately 55 a/o iron, that is, near the composition of the congruent maximum of the sigma phase. However, in view of the nonconfigurational factors that appear to dominate the excess entropies and the enthalpies, it is not believed that the excess free energies can be considered simply in terms of a tendency toward compound formation.(42)

Although the values of the excess free energies are regarded as more reliable, the values of the excess entropies are more amenable to discussion. The zero-point entropy of an ideally behaved binary alloy is given by equations (39) and (54). However, most alloys tend to deviate significantly from ideal behavior, particularly at elevated temperatures, which gives rise to an entropy that may be either greater or less than the ideal entropy. This deviation expressed in terms of the excess entropy is defined by the relationship

$$\Delta S^{ex} = \Delta S - \Delta S^{id} \quad . \tag{63}$$

The excess entropy of formation may be correlated with the nonideal changes that occur in the atomic and electronic structures of the component metals upon alloying, as manifested by the configurational, vibrational, and magnetic characteristics of the alloys.

The configurational contribution to the excess entropy must of necessity be negative since departures from completely random mixing, whether towards short-range ordering or clustering, will result in entropies whose values are lower than ideal. In the vanadium-iron alloy system, the existence of an extensive series of disordered b.c.c. solid solutions at 1600°K implies that this contribution should be very small, although the occurrence at lower temperatures of CsCl-type order in the alpha phase, and at higher temperatures of a liquidus-solidus minimum, suggests that some nonrandomness may exist in the alloys at 1600°K.

The vibrational entropy, which is associated with the change in the atomic and electronic bonding characteristics upon alloying, is expressed by the relationship

$$\Delta S^{ex}_{vib} = \int_0^T \Delta C_p \, d \ln T \quad , \tag{64}$$

where ΔC_p represents the deviation of the atomic and electronic specific heats from Neumann-Kopp behavior. Although no high-temperature specific heats have been measured in this system, an approximate evaluation of this relation may be made near room temperature by means of the

Debye theory of heat capacity and the Debye temperatures and electronic specific heat coefficients determined by Cheng et al.[63] The entropies thus calculated, listed in Table XXI, are mainly negative. The negative departures from ideality are in qualitative agreement with the negative deviations of the room-temperature lattice parameters from Vegard's law[64,65] and the decrease in the diffusion rates of a number of solute elements into vanadium-iron alloys as compared with pure iron.[66] However, it has been suggested[67] that deviations from Neumann-Kopp behavior become more positive as melting temperatures are approached. This is particularly true when a minimum occurs in the liquidus-solidus, as a minimum signifiies that the deviations of the activities from ideality in the solid are more positive than in the liquid. The expected misfit energy in the solid leads to an increase in the vibrational frequencies compared to the pure components.[68] Hume-Rothery and Christian[69] believe that the differences in Pauling valence between vanadium and iron are sufficient to explain this slight tendency toward phase separation. Thus, the vibrational entropy at high temperatures (1600°K) may in fact be positive with a maximum value at the composition of the liquidus-solidus minimum, in spite of the indications that at lower temperatures it is negative. It is difficult to assess the integrated contribution to the excess entropy that arises from the small disparities in atomic size, valence, and electronegativity that exist between the component metals. Whereas differences in atomic size give rise to positive contributions to ΔS^{ex}_{vib}, a difference in electronegativity gives rise to negative contributions. Finally, an inequality in the valence often produces an asymmetry in the plot of entropy versus composition.[61]

Table XXI

COMPUTED VALUES OF THE VIBRATIONAL ENTROPY AND ENTHALPY OF FORMATION AT 298°K*

N_{Fe}	$\Delta S^{ex}_{vib\ at}$	$\Delta S^{ex}_{vib\ el}$	$\Delta H_{vib\ at}$	$\Delta H_{vib\ el}$
	cal/(gm-atom)(deg)		cal/gm-atom	
1.0	0.00	0.00	0.0	0.0
0.67	+0.38	-0.189	+44.8	-42.4
0.45	-1.26	-0.117	-130.5	-17.4
0.34	-0.38	-0.0398	-31.4	-5.9
0.20	-2.23	-0.297	-241.9	-44.2
0.15	-2.12	-0.220	-224.5	-32.8
0.08	-1.33	-0.130	-131.0	-19.3
0.0	0.00	0.00	0.0	0.0

*Assuming Cp ≈ Cv.

The magnetic entropy is dependent upon the degree of randomness in the orientation of the atomic magnetic moments that are associated with the iron atoms in all but the vanadium-rich alloys.[62,70] Above the Curie temperature, the total entropy of hypothetical paramagnetic iron with no atomic moments is lower than that of paramagnetic iron with randomly oriented moments by an amount R ln (μ_B + 1) = 2.3 cal/(gm-atom)(deg).[44,71] Here, μ_B is equal to 2.2 in Bohr magnetons, the average atomic magnetic moment per iron atom. Upon alloying either of these two forms of paramagnetic iron with vanadium, which has been assumed to carry no magnetic moment,[72,73] ideal behavior occurs insofar as the magnetic entropy is concerned, when the magnetic moment per iron atom remains constant, at either 0 or 2.2. These two ideal states are illustrated by the dashed lines in Figure 20. Neither of these relations is to be expected in the real alloys, as the paramagnetic moment per iron atom in iron-vanadium alloys gradually decreases with increasing vanadium concentration and disappears at about 22 a/o Fe.[63,73,74] The resultant magnetic entropy should be approximated by the solid line in Figure 20.

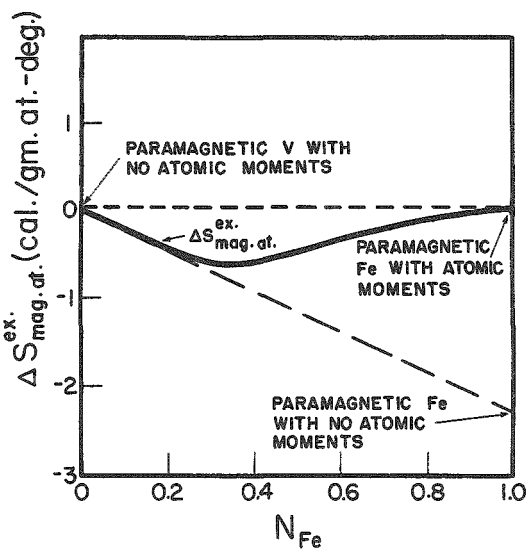

35293

Figure 20. Plot of ΔS^{ex}_{mag}

An alteration in the character of the electron wave functions upon alloying may make a contribution to the entropy. One of the contributions to the Knight shift in vanadium-iron alloys has been considered as evidence that the number of electrons at the Fermi surface whose wave functions have s character increases relative to those with non-s character from pure vanadium and reached a maximum around 16 a/o Fe.[74-76] Since the spatial distributions of the probability densities of s-electron wave functions are more random than for non-s-electron wave functions,[77] a small positive contribution might be made to the entropy with a maximum at 16 a/o Fe.

A further possible contribution to the entropy may arise from the degree of localization of the d-electron wave functions at the iron atoms. As the wave functions become less localized, their probability densities become more randomly distributed throughout the lattice and, presumably, represent a configuration with higher entropy. Cheng et al.[63] have stated that the d-electron wave functions show relatively little tendency to be localized at the iron atoms in the vanadium-rich alloys, but that beyond 22 a/o Fe a tendency for localization is clearly indicated. Because the degree of localization does not remain constant when vanadium and iron are alloyed, that is, the alloys do not behave ideally, a small positive contribution, which has a maximum at 22 a/o Fe, might be made to the entropy.

In summary, the positive excess entropies found experimentally have the wrong sign to be either configurational or magnetic in origin. There is some basis for the belief that a strong vibrational contribution may be made at elevated temperatures. The changes in the electronic configurations of the components that occur on alloying could also contribute to the excess entropy, although no theoretical basis has yet been put forward.

The enthalpies of formation are also composed of several additive terms related to the changes that occur in the atomic and electronic structures of the component metals upon alloying.

According to the usual nearest-neighbor approximations,[78] the configurational contribution to the enthalpy may be expressed in terms of the pairwise bond energies E between nearest neighbors. In a binary alloy that exhibits some degree of clustering, E_{12} is less than $\frac{1}{2}(E_{11} + E_{22})$ and the enthalpy is positive;[79] similarly, if ordering occurs, E_{12} is greater than $\frac{1}{2}(E_{11} + E_{22})$ and the enthalpy is negative. Hence, at 1600°K the small configurational enthalpy term may be positive at the composition of the liquidus-solidus minimum and negative near the equiatomic composition.

The vibrational enthalpy is related to the thermal excitation of atoms and electrons by the relationship

$$\Delta H_{vib} = \int_0^T \Delta C_p dT \quad . \tag{65}$$

Both the Debye temperatures and the electronic specific heat coefficients indicate that the deviations from Neumann-Kopp behavior at about room temperature are negative; this leads to negative thermal enthalpies (see Table XXI). However, at elevated temperatures the occurrence of a liquidus-solidus minimum suggests the existence of a misfit energy in the solid alloys. Wagner[80] has derived an equation for calculating the difference in excess free energies between the solid and liquid state at such a minimum from a knowledge of the phase diagram and the entropies of fusion of the pure components. A value of +370 cal/gm-atom is obtained for this difference in the vanadium-iron alloy system. If the entropy change on melting is assumed to be small, then the thermal enthalpy is approximately +370 cal/gm-atom at the liquidus-solidus minimum. Hence, there is some basis for positive values of the vibrational enthalpy at 1600°K.

The magnetic and electronic contributions to the enthalpy could be discussed in a manner similar to the contribution to the entropy, but the theoretical basis is not as well established. However, since these terms affect the heat capacity, the signs of the related entropy and enthalpy contributions must be the same.

Although the activities and free energies of formation obtained at 1600°K appear to be reliable and self-consistent, the entropies and enthalpies of formation are considerably more difficult to rationalize. The apparent positive excess entropies and enthalpies have been discussed in terms of the known properties of the alloy system. The present work tends to demonstrate the importance of nonconfigurational contributions to the thermodynamic properties of transition metal alloys. Further elucidation of the thermodynamics of the vanadium-iron alloy system must await direct measurements of the enthalpies of formation and high-temperature heat capacities.

The only previous thermodynamic study of the vanadium-iron alloy system was made by Saxer,[54] who used the Knudsen effusion method over the temperature range from 1550 to 1725°K. In this study, the activities of iron exhibit a negative deviation from Raoult's law but tend to approach ideality as the temperature is raised. The calculated activities of vanadium also show negative deviations in the iron-rich alloys but approach Raoultian behavior in the vanadium-rich alloys. From these activities, values of the free energy of formation are computed. Heats of formation determined by means of the second law of thermodynamics are found to be negative. Integral values of the free energies, entropies, and heats of formation in the vanadium-iron alloy system at 1613°K as reported by Saxer are plotted in Figure 21.

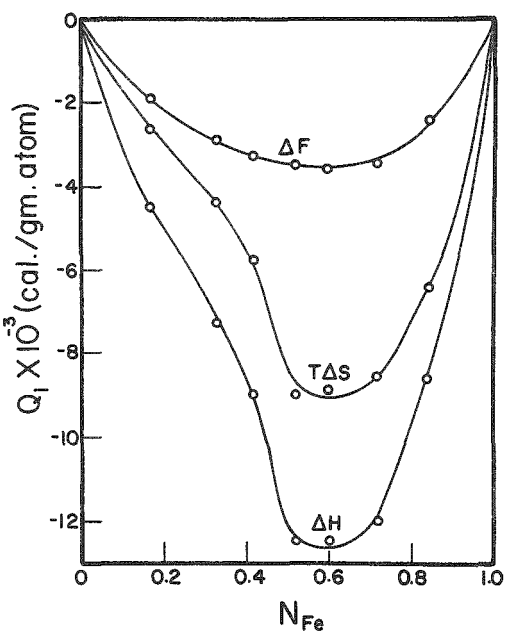

34894

Figure 21. Integral Free Energies, Entropies, and Heats of Formation in the Vanadium-Iron Alloy System at 1613°K after Saxer[54]

Before discussing the disagreement among the entropies and enthalpies of formation as calculated by Saxer and by the present work, it should first be noted that good accord does exist among the free energies of formation, as shown in Figures 15 and 21. This agreement suggests that the temperature coefficients of the activities, which were determined by the two studies, must be critically evaluated. The temperature coefficients of the activity of a component of an alloy is directly related to the ratio between the slope of the log p_{Fe} vs $1/T$ curve of the alloy to that of pure iron. As seen in Figure 22 and in Figure 10, the slopes of the vapor pressure curves as found by Saxer increase relative to that of pure iron as compared with the present work, in which the slopes in general decrease relative to that of pure iron. It is difficult to isolate the source of these differences in the relative slopes. However, the two most likely sources are a systematic

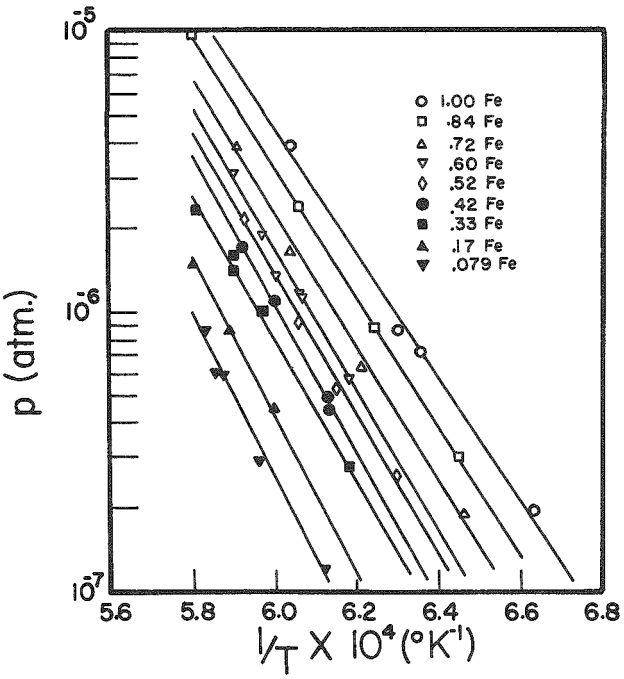

34989

Figure 22. Vapor Pressure Curves of Vanadium-Iron Alloys after Saxer[54]

error in the measurement of the temperature of the effusion cell and the precision of the slopes of the vapor pressure curves, which were determined by a least-squares treatment of the data. In the present work, considerable attention has been given to the temperature calibration of the effusion cells. Saxer, on the other hand, does not describe in detail either the calibration of the optical pyrometer he used or the accuracy of his temperature measurements. The small degree of scatter in the data of the present research and the number of data points, as seen in Figure 9, lead to a reliable evaluation of the slopes of the vapor pressure curves by the least-squares method. Alternatively, the considerable degree of scatter in the data as determined by Saxer and the limited number of data points, as seen in Figure 22, do not seem to permit such an evaluation.

The large negative values of the enthalpies of formation, which were found by Saxer, are implausible when compared with enthalpy data for other alloy systems. These values are at least twice as large as any other values with the exception of some alloy systems in which intermetallic compounds are formed or where the component metals are widely separated in the periodic table, for example potassium-mercury.[81]

Conclusions

In the present investigation, the vapor pressures of pure iron and iron over vanadium-iron alloys have been measured with the torsion-effusion apparatus. Reliable thermodynamic values of the free energies of formation of vanadium-iron alloys have been determined. The entropies and enthalpies of formation of the same alloys have been calculated from the temperature coefficients of the activities. The apparent positive excess entropies and enthalpies have been discussed in terms of the known properties of the alloy system. The present work demonstrates the importance of the contributions that the nonconfigurational terms make to the thermodynamic properties of transition metal alloys.

As a result of the conflicting values for the excess entropies of formation as found by Saxer and as determined in this present work, it is proposed that a calorimetric determination be made of the enthalpies of formation of these alloys. These enthalpy data when combined with the free energy data found in this present study would permit an unambiguous evaluation of the entropy of formation. It is also suggested that experiments be performed in additional alloy systems, such as the manganese-vanadium system, that might provide for a clearer delineation of the various contributions to the excess entropy of formation.

REFERENCES

1. F. E. Wittig, Paper 1A, N.P.L. Symposium No. 9, The Physical Chemistry of Metallic Solutions and Intermetallic Compounds. H.M.S.O., London (1959).
2. J. Chipman, J. F. Elliott, and B. L. Averbach, Paper 1B, N.P.L. Symposium No. 9, The Physical Chemistry of Metallic Solutions and Intermetallic Compounds. H.M.S.O., London (1959).
3. R. W. Ditchburn and J. C. Gilmour, Rev. Mod. Phys., 13, 310 (1941).
4. O. Kubaschewski and E. Ll. Evans, Metallurgical Thermochemistry, Pergamon Press Inc., New York (1958).
5. I. Langmuir, Phys. Rev., 2, 329 (1913).
6. M. Knudsen, Ann. Phys., 28, 75 (1909).
7. M. Knudsen, Ann. Phys., 29, 179 (1909).
8. R. Speiser and J. W. Spretnak, "Determination of the Vapor Pressure of Metals and Alloys," Vacuum Metallurgy, Electrochemical Society, Inc. (1955).
9. C. I. Whitman, J. Chem. Phys., 20, 161 (1951).
10. C. I. Whitman, J. Chem. Phys., 21, 1407 (1953).
11. P. Clausing, Ann. Phys., 12, 961 (1932).
12. S. Dushman, Scientific Foundations of Vacuum Technique, John Wiley and Sons, Inc., New York (1959).
13. H. Mayer, Z. Phys., 67, 240 (1931).
14. M. Volmer, Z. Phys. Chem. (Bodenstein Festband, 1931 Suppl.), 863 (1931).
15. K. Neumann and E. Volker, Z. Phys. Chem. A161, 33 (1932).
16. R. D. Freeman and A. W. Searcy, J. Chem. Phys., 22, 762 (1954).
17. D. A. Schulz and A. W. Searcy, J. Chem. Phys., 36, 3099 (1962).
18. S. P. Detkov, Zhur. Fiz. Khim., 34, 1634 (1960).
19. M. Hansen, Constitution of Binary Alloys, McGraw-Hill Book Co., Inc., New York (1958).
20. K. Neumann and E. Lichtenberg, Z. Phys. Chem. A184, 89 (1939).
21. K. Niwa and M. Yosiyama, J. Fac. Sci. Hokkaido Imp. University. Ser. III, 3, 75 (1940).
22. K. Niwa and Z. Sibata, J. Chem. Soc. Japan, 61, 667 (1940).
23. K. Niwa, J. Chem. Soc. Japan, 61, 770 (1940).

24. K. Niwa and M. Yosiyama, J. Chem. Soc. Japan, 61, 1055 (1940).

25. M. Yosiyama, J. Chem. Soc. Japan, 62, 204 (1941).

26. G. Wessel, Z. Phys., 130, 539 (1951).

27. A. W. Searcy and R. D. Freeman, J. Amer. Chem. Soc., 76, 5229 (1954).

28. A. W. Searcy and R. D. Freeman, J. Chem. Phys., 23, 88 (1955).

29. R. F. Barrow, P. G. Dodsworth, A. R. Downie, E.A.N.S. Jeffries, A.C.P. Pugh, F. J. Smith, and J. M. Swinstead, Trans. Farad. Soc., 51, 1354 (1955).

30. A. Roeder and W. Morawietz, Z. Elektrochem., 60, 431 (1956).

31. A.C.P. Pugh and R. F. Barrow, Trans. Farad. Soc., 54, 671 (1958).

32. A. T. Aldred, J. D. Filby, and J. N. Pratt, Trans. Farad. Soc., 55, 2030 (1959).

33. A. T. Aldred and J. N. Pratt, Trans. Farad. Soc., 57, 611 (1961).

34. G. M. Rosenblatt and C. E. Birchenall, J. Chem. Phys., 35, 788 (1961).

35. C. L. Rosen, Rev. Sci. Instr., 31, 837 (1960).

36. J. N. Pratt and A. T. Aldred, J. Sci. Instr., 36, 465 (1959).

37. F. B. Seely and N. E. Ensign, Analytical Mechanics for Engineers, John Wiley and Sons, Inc., New York (1953).

38. J. W. Edwards, R. Speiser, and H. L. Johnston, J. Appl. Phys., 22, 424 (1951).

39. M. Knudsen, Kinetic Theory of Gases, John Wiley and Sons, Inc., New York (1950).

40. K. D. Carlson, The Molecular and Viscous Effusion of Saturated Vapors, ANL-6156, (1960).

41. S. Glasstone, Thermodynamics for Chemists, D. Van Nostrand Co., Inc., Princeton, N. J. (1958).

42. L. S. Darken and R. W. Gurry, Physical Chemistry of Metals, McGraw-Hill Book Co., Inc., New York (1953).

43. J. C. Fisher, Trans. AIME, 185, 688 (1949).

44. R. J. Weiss and K. J. Tauer, Phys. Rev., 102, 1490 (1956).

45. H. A. Jones, I. Langmuir, and G. M. J. Mackay, Phys. Rev., 30, 201 (1927).

46. A. L. Marshall, R. W. Dornte, and F. J. Norton, J. Am. Chem. Soc., 59, 1161 (1937).

47. J. W. Edwards, H. L. Johnston, and W. E. Ditmars, J. Am. Chem. Soc., 73, 4729 (1951).

48. V. D. Burlakov, Fiz. Met. i Metall., 5, 91 (1957).

49. Yu. V. Kornev and V. N. Golubkin, Fiz. Met. i Metall., 1, 286 (1955). AEC-TR-2924 (1958).

50. E. A. Gulbransen and K. F. Andrew, Trans. AIME, 221, 1247 (1961).

51. E. Z. Vintaikin, Doklady Akad. Nauk S.S.S.R., 117, 632 (1957).

52. L. I. Ivanov and M. P. Matveeva, Trudy Inst. Met. in A. A. Baikova, 1, 104 (1957).

53. R. Speiser, A. J. Jacobs, and J. W. Spretnak, Trans. AIME, 215, 185 (1959).

54. R. K. Saxer, The Chemical Activities of Iron and Vanadium in Binary Iron-Vanadium Alloys and the Vapor Pressures of Pure Cobalt, Iron, and Vanadium, The Ohio State University, Columbus, Ohio (1962), A Thesis.

55. C. L. McCabe, R. G. Hudson, and H. W. Paxton, Trans. AIME, 212, 102 (1958).

56. A. Goldsmith, T. E. Waterman, and H. J. Hirschhorn, Handbook of Thermophysical Properties of Solid Materials, Vol. I, The Macmillan Co., New York (1961).

57. R. Hultgren and Associates, Thermodynamic Properties of Metals and Alloys, Minerals Research Laboratory, Inst. of Eng. Res., Univ. of Calif., Berkeley, Calif. (1961 revision).

58. A. N. Nesmeyanov, B. Z. Iofa, and B. V. Karasev, Doklady Akad. Nauk S.S.S.R., 112, 882 (1957).

59. D. R. Stull and G. C. Sinke, Thermodynamic Properties of the Elements, American Chemical Society, Washington, D. C. (1956).

60. R. A. Oriani, Paper 2A, N.P.L. Symposium No. 9, The Physical Chemistry of Metallic Solutions and Intermetallic Compounds, H.M.S.O., London (1959).

61. O. J. Kleppa, Paper contributed to Colloquium on "The Structure of Metallic Solid Solutions" Orsay (France), July 9-11 (1962).

62. R. A. Oriani and W. K. Murphy, Acta. Met., 10, 879 (1962).

63. C. H. Cheng, C. T. Wei, and P. A. Beck, Phys. Rev., 120, 426 (1960).

64. H. Martens and P. Duwez, Trans. Am. Soc. Metals, 44, 484 (1952).

65. A. L. Sutton and W. Hume-Rothery, Phil. Mag., 46, 1295 (1955).

66. M. A. Krishtal, Fiz. Met. i Metall., 9, 680 (1960).

67. R. A. Oriani, Acta Met., 3, 232 (1955).

68. L. L. Seigle, M. Cohen, and B. L. Averbach, J. Met., 4, 1320 (1952).

69. W. Hume-Rothery and J. W. Christian, Phil. Mag., 36, 835 (1946).

70. S. V. Radcliffe, B. L. Averbach, and M. Cohen, Acta Met., 9, 169 (1961).

71. R. A. Oriani, J. Chem. Phys., 28, 679 (1958).

72. M. V. Nevitt and A. T. Aldred, J. Appl. Phys., 34, 463 (1963).

73. S. Arajs, R. V. Colvin, H. Chessin, and J. M. Peck, J. Appl. Phys., 33, 1353 (1962).

74. D. J. Lam, D. O. Van Ostenburg, H. D. Trapp, and D. W. Pracht, (to be published).

75. D. J. Lam, D. O. Van Ostenburg, H. D. Trapp, and D. E. MacLeod, J. Met., 14, 601 (1962).

76. D. O. Van Ostenburg, D. J. Lam, H. D. Trapp, and D. E. MacLeod, Phys. Rev., 128, 1550 (1962).

77. W. R. Trost, Orbital Theory in the Transition Metals, R42, Dept. of Mines and Technical Surveys, Ottawa (1958).

78. R. Fowler and E. A. Guggenheim, Statistical Thermodynamics, Cambridge University Press, Cambridge, England (1949).

79. R. A. Oriani, Acta Met., 1, 448 (1953).

80. C. Wagner, Thermodynamics of Alloys, Addison-Wesley Press, Inc., Cambridge, Mass. (1952).

81. O. Kubaschewski, and J. A. Catterall, Thermochemical Data of Alloys, Pergamon Press Inc., New York (1956).

ACKNOWLEDGMENT

The author is grateful to Professor R. W. Bohl of the University of Illinois for his continued interest and helpful discussions in the course of this investigation.

He wishes to express his appreciation to M. V. Nevitt of the Argonne National Laboratory for his advice, encouragement, and assistance.

Special thanks must also be given to A T. Aldred of the Argonne National Laboratory who suggested the general subject of this thesis and whose enthusiasm and practical understanding of thermodynamic research continued to stimulate the author.

This report is based on a thesis written at the Argonne National Laboratory under the auspices of the U.S. Atomic Energy Commission under a cooperative arrangement with the Department of Mining, Metallurgy, and Petroleum Engineering of the University of Illinois, Urbana, Illinois.